DEVELOPMENT AND IMPLEMENTATION OF A LOCAL ALGEBRAIC TRANSITION MODEL IN k-ω-SST FORMULATION

A THESIS SUBMITTED TO
THE GRADUATE SCHOOL OF NATURAL AND APPLIED SCIENCES
OF
MIDDLE EAST TECHNICAL UNIVERSITY

BY

BİLAL OKUMUŞ

IN PARTIAL FULFILLMENT OF THE REQUIREMENTS
FOR
THE DEGREE OF MASTER OF SCIENCE
IN
MECHANICAL ENGINEERING

AUGUST 2023

Approval of the thesis:

DEVELOPMENT AND IMPLEMENTATION OF A LOCAL ALGEBRAIC TRANSITION MODEL IN k-ω-SST FORMULATION

submitted by **BİLAL OKUMUŞ** in partial fulfillment of the requirements for the degree of **Master of Science in Mechanical Engineering Department, Middle East Technical University** by,

Prof. Dr. Halil Kalıpçılar
Dean, Graduate School of **Natural and Applied Sciences** _____

Prof. Dr. Mehmet Ali Sahir Arıkan
Head of Department, **Mechanical Engineering** _____

Assist. Prof. Dr. Özgür Uğraş Baran
Supervisor, **Mechanical Engineering, METU** _____

Assist. Prof. Dr. Onur Baş
Co-supervisor, **Mechanical Engineering, TEDU** _____

Examining Committee Members:

Prof. Dr. Mehmet Metin Yavuz
Mechanical Engineering, METU _____

Assist. Prof. Dr. Özgür Uğraş Baran
Mechanical Engineering, METU _____

Assist. Prof. Dr. Onur Baş
Mechanical Engineering, TEDU _____

Prof. Dr. Hakan Ertürk
Mechanical Engineering, Bogazici University _____

Assist. Prof. Dr. Sıtkı Uslu
Mechanical Engineering, TOBB ETU _____

Date: 17.08.2023

I hereby declare that all information in this document has been obtained and presented in accordance with academic rules and ethical conduct. I also declare that, as required by these rules and conduct, I have fully cited and referenced all material and results that are not original to this work.

Name, Surname: BİLAL OKUMUŞ

Signature :

ABSTRACT

DEVELOPMENT AND IMPLEMENTATION OF A LOCAL ALGEBRAIC TRANSITION MODEL IN K-ω-SST FORMULATION

OKUMUŞ, BİLAL
M.S., Department of Mechanical Engineering
Supervisor: Assist. Prof. Dr. Özgür Uğraş Baran
Co-Supervisor: Assist. Prof. Dr. Onur Baş

August 2023, 72 pages

This study proposes a new correlation-based algebraic transition model using local variables. Instead of solving an additional transport equation for intermittency, the model employs an intermittency function that controls the source terms of the turbulence model used. Thus, the new model solves transition problems using much less computational power compared to one- or two-equation transition models. The intermittency function of the present model is a more sophisticated modified version of that in the SA-BCM transition model, and it is coupled with the k-ω-SST turbulence model to eliminate the shortcomings in the SA-BCM model. The present model is implemented in an in-house CFD solver and calibrated against a series of standard flat plate experiments. An additional airfoil test case is used to calibrate the parameter that provides separation correction. The model is tested with remaining flat plate and airfoil test cases. The validation results show a good agreement with the experiments. It is shown that the new model provides comparable success with more complicated transition models. Therefore, the present model provides an alternative means to include boundary layer transition effects in CFD simulations by reducing the number

of constants and functions needed compared to that in other transition models.

Keywords: Laminar-to-turbulent Transition, Correlation-based Transition Model, Turbulence Modeling, Algebraic Model, Intermittency Function

ÖZ

K-ω-SST MODELİ İÇİN YEREL CEBİRSEL TÜRBÜLANSA GEÇİŞ MODELİ GELİŞTİRİLMESİ VE UYGULANMASI

OKUMUŞ, BİLAL
Yüksek Lisans, Makina Mühendisliği Bölümü
Tez Yöneticisi: Dr. Öğr. Üyesi. Özgür Uğraş Baran
Ortak Tez Yöneticisi: Dr. Öğr. Üyesi. Onur Baş

Ağustos 2023 , 72 sayfa

Bu çalışmada, yerel değişkenleri kullanan korelasyon tabanlı yeni bir cebirsel türbülansa geçiş modeli sunulmaktadır. Model, kesiklilik için fazladan bir taşınım denklemi çözmek yerine, kullanılan türbülans modelinin üretim terimini kontrol eden bir kesiklilik fonksiyonundan faydalanmaktadır. Böylece model, bir veya iki denklemli modellere göre çok daha az hesaplama gücü kullanarak problemleri çözmeyi başarmaktadır. Modelin kesiklilik fonksiyonu, SA-BCM türbülansa geçiş modelindeki fonksiyonun oldukça geliştirilip değiştirilmiş bir hâlidir ve SA-BCM modelindeki eksiklikleri ortadan kaldırmak için k-ω-SST türbülans modeli ile birleştirilmiştir. Mevcut model, kurum içi geliştirilen bir HAD çözücüsüne eklenip standart düz levha deneyleri kullanılarak kalibre edilmiştir. Akım ayrışması ihtiva eden geçiş problemleri içi ek bir parametre de 2 boyutlu kanat deney sonuçları kullanılarak kalibre edilmiştir. Geliştirilen model diğer düz levha ve kanat deneyleri ile doğrulanmıştır. Yeni model ile alınan benzetimler sonucu deneylerle uyumlu sonuçlar elde edilmiştir. Böylece yeni modelin daha karmaşık türbülans geçiş modelleri ile benzer sonuçlar

verdiği gösterilmiştir. Buna göre, mevcut model, diğer türbülansa geçiş modellerindekine kıyasla ihtiyaç duyulan sabit ve fonksiyonların sayısını azaltarak, türbülansa geçiş etkilerini HAD benzetimlerine dahil etmek için alternatif bir yol sağlamaktadır.

Anahtar Kelimeler: Türbülansa Geçiş, Korelasyon Tabanlı Geçiş Modeli, Türbülans Modelleme, Cebirsel Model, Kesiklilik Fonksiyonu

To my family

ACKNOWLEDGMENTS

First and foremost, I offer my deepest gratitude to my thesis advisors, Dr. Özgür Uğraş Baran and Dr. Onur Baş, for their guidance, invaluable feedback, constructive criticism, and continuous encouragement throughout the research. Their mentorship has enriched my understanding of the subject and has given me the strength to try again and again.

I am profoundly thankful to my beloved wife, Cansel Şener Okumuş, whose unwavering support has been a constant source of motivation for me. She has always been the one to stand by me through any challenges.

I am also deeply indebted to my parents for their encouragement and unconditional belief in me. I would not have achieved any success without them.

Finally, I would like to express my gratitude to the late Dr. Cemil Yamalı, whose inspiring thermodynamics lectures were the driving force of my curiosity in fluid mechanics. May he rest in peace.

TABLE OF CONTENTS

LIST OF TABLES

TABLES

LIST OF FIGURES

FIGURES

LIST OF SYMBOLS

Greek symbols

γ	Intermittency factor
δ	Boundary layer thickness
ϵ	Turbulence dissipation rate
θ	Momentum thickness
λ	Pressure gradient parameter
μ	Dynamic viscosity
μ_t	Dynamic eddy-viscosity
ν	Kinematic viscosity
ν_t	Kinematic eddy-viscosity
$\tilde{\nu}$	Working variable of SA model
ρ	Density
τ	Shear stress
ϕ	Intermittency function
ω	Specific turbulence dissipation rate
Ω	The magnitude of the vorticity rate

Latin characters

AoA	Angle of attack (deg.)
c	Chord length
c_d	Drag coefficient
c_f	Skin friction coefficient
c_l	Lift coefficient
c_p	Pressure coefficient
d_w	Minimum wall distance
h	Grid spacing
H	Shape factor
k	Turbulence kinetic energy
k_L	Laminar kinetic energy
k_T	Turbulence kinetic energy
M	Mach number
N	Global amplification factor
$\tilde{n}$	Global amplification factor of the AFT model
p	Pressure
P_t	Total pressure
Re	Reynolds number
Re_θ	Momentum thickness Reynolds number
$Re_{\theta c}$	Critical momentum thickness Reynolds number

$Re_{\theta t}$ Transition onset momentum thickness Reynolds number

$\widetilde{Re_{\theta t}}$ Local transition onset momentum thickness Reynolds number (obtained from a transport equation)

Re_T Turbulent Reynolds number

Re_v Vorticity Reynolds number

S The magnitude of the strain rate

Tu Turbulence intensity (%)

U Velocity

x, y, z Cartesian components

x_t Transition location

y^+ Nondimensional wall distance

Subscripts

∞ Free-stream

PG Pressure gradient

L Local

LE Leading edge

Abbrevations

AFT Amplification Factor Transport

CFD Computational Fluid Dynamics

DNS Direct Numerical Simulation

$ERCOFTAC$ European Research Community on Flow, Turbulence and Combustion

$FSTI$ Free-Stream Turbulence Intensity

$HLLC$ Harten-Lax-van Leer-Contact

$LCTM$ Local Correlation-Based Transition Modeling

LES Large Eddy Simulation

LKE Laminar Kinetic Energy

LSB Laminar Separation Bubble

$LSGS$ Line-Symmetric Gauss-Seidel

$MUSCL$ Monotonic Upstream-centered Scheme for Conservation Laws

$NASA$ National Aeronautics and Space Administration

$RANS$ Reynolds-Averaged Navier-Stokes

SA Spalart-Allmaras

$SA-BC$ Spalart-Allmaras-Bas-Cakmakcioglu

$SA-BCM$ Spalart-Allmaras-Bas-Cakmakcioglu with Modifications

SST Shear Stress Transport

$S\&K$ Schubauer and Klebanoff

$T-S$ Tollmien-Schlichting

CHAPTER 1

INTRODUCTION

Boundary layer transition to turbulence is widely encountered in today's industrial CFD problems. Its application areas vary from low Reynolds number flows on aerial vehicles to turbomachinery flows [1]. The complexity of the transition, which has distinct mechanisms compared to turbulence, makes it difficult to model with a unified equation. The primary approach in CFD modeling remained to assume the flow is fully turbulent, neglecting the transition process [2]. DNS is an alternative, but today's computational resources are still insufficient for its general industry use. Therefore, transition-aware model development has been an active research topic for decades and much progress has been made from stability theory-based methods such as the e^N method [3, 4] to the Local Correlation-Based Transition Modeling (LCTM) concept [5, 2, 6, 7, 8].

Historically, the earlier method used to model the transitional effects is the e^N method [3, 4]. Although this method gives reasonably good results in predicting natural transition, it fails when the domain is subjected to high freestream turbulence intensity [8]. Due to high freestream turbulence intensity, the transition mechanism is no longer the natural transition but becomes the bypass transition. As the linear instability stages are *bypassed*, the stability theory-based methods have no capability to predict bypass transition. In addition, the e^N method requires coupling with a high-resolution boundary layer code and solving numerous non-local operations that cannot be easily performed by modern general-purpose CFD codes [8].

Low Reynolds number turbulence models are another method of choice. These models try to reproduce laminar behavior near the wall by means of damping functions [9]. However, they suffer from the lack of representing real flow physics and are

found to be unreliable [6].

A major milestone in transition modeling is the introduction of the *intermittency* concept in the model equations, based on Emmons' [10] ideas of the random intermittent characteristics of turbulence. Emmons [10] proposed a probability distribution function for turbulence called *intermittency factor,* γ. This factor takes a value of zero in the laminar flow regime, while it becomes one when the flow turns completely turbulent. The values between 0 and 1 are transitional flows that are entirely not laminar or turbulent. Later, Dhawan and Narasimha [11] improved the formulation of the intermittency factor by using a wide range of experiments and suggested a generalized intermittency function related to turbulent spot production rate and transition location. Starting from this, Steelant and Dick [12] and, following, Suzen and Huang [13] developed a transport equation for intermittency to reproduce the intermittency profile of Dhawan and Narasimha [11]. They also coupled this intermittency equation with two-equation turbulence models to manipulate turbulence production. Although promising results were obtained, the implementation and utilization of these models were not straightforward.

The essential difficulty in intermittency-based methods stems from their need for non-local information, i.e., information transfer from non-adjacent cells, to evaluate whether the transition criterion is met. The transition location in intermittency-based models is usually determined through experimental correlations such as those of Abu-Ghannam and Shaw [14] or Mayle [15]. Correlations provide the transition momentum thickness Reynolds number $Re_{\theta t}$ at which the transition occurs, and the models try to find the location where the local momentum thickness Reynolds number Re_θ exceeds the critical value. That process has the following problematic aspects:

1. Momentum thickness Reynolds number is an integral boundary layer parameter, so taking integrals normal to the walls is required to evaluate it. However, taking integrals is not an easy task to do in the framework of modern general-purpose CFD codes using unstructured grids and relying on parallel execution [8] due to the necessity to implement additional search and integration algorithms for complex geometries [16].

2. Correlations depend on freestream turbulence intensity. Although it does not

pose a big problem as much as the previous item, a non-local information transfer is again needed. However, if freestream turbulence intensity is not a constant but a locally calculated variable, a violation of the Galilean-invariance principle is introduced, as the turbulence intensity depends on the velocity.

To avoid the former drawback, Menter et al. [5] presented a novel approach suggesting that a local scaled parameter, vorticity (or strain rate) Reynolds number Re_v [17], could be used to estimate the momentum thickness Reynolds number Re_θ. They proposed an intermittency transport equation whose transition onset function depends on the proportionality of vorticity Reynolds number Re_v and critical momentum thickness Reynolds number $Re_{\theta c}$ obtained from correlations. As for the latter drawback, they proposed another transport equation to use local freestream parameters in the correlations. Thus, they overcame the non-information transfer issues, although the Galielan-invariance problem remained. This complete model, called the γ-$\widetilde{Re_{\theta t}}$ model, was a substantial leap forward in transition modeling as an entirely local formulation was achieved for a correlation-based transition model. Menter et al. [7] named the modeling framework based on these ideas as *Local Correlation-Based Transition Modeling (LCTM)*.

The γ-$\widetilde{Re_{\theta t}}$ model is validated by different research groups [18] and has shown its success in general applications [19]. On the other hand, the γ-$\widetilde{Re_{\theta t}}$ model is quite complex and computationally demanding. It involves a series of functions and constants besides the correlations, and two additional transport equations are required to be solved. These significantly increase the computational cost. Moreover, the calibration way used in the model is not safe as a high number of constants are calibrated based on the limited test cases.

Baş et al. [20] suggested a pragmatic idea that it is not strictly necessary to have an additional equation to convect and diffuse the intermittency through the domain. Because there already exists an equation that has convection and diffusion terms, and it is the turbulence equation. Starting from this point, they coupled the Spalart-Allmaras turbulence model [21] with an intermittency function that turns on the production term of the turbulence equation when the critical momentum thickness Reynolds number based on experimental correlation is exceeded and, otherwise, turns it off.

The combined model is called the SA-BC transition model [20, 16], and later with further improvements, the SA-BCM model [22, 23]. Although the SA-BC model relied on a very simple idea and its intermittency function had only two controlling parameters, the model showed promising results compared to higher-order transition models [24].

Meanwhile, some attempts to simplify the γ-$\widetilde{Re_{\theta t}}$ model were made. Coder and Maughmer [25] suggested a correlation derived using a non-dimensional local pressure-gradient parameter to eliminate the $\widetilde{Re_{\theta t}}$ equation. Later, Menter et al. [2] proposed the γ model by dropping the $\widetilde{Re_{\theta t}}$ equation and adjusting the functions and coefficients. They simplified the correlations in the γ-$\widetilde{Re_{\theta t}}$ model by suggesting local turbulence intensity and pressure gradient formulations. Thus, the use of freestream velocity in the onset correlation is avoided, and the Galilean-invariance problem is solved. The additional transport equation for intermittency, however, could not be dropped until recently. Sandhu and Ghosh [26] performed a sophisticated modification on the γ model [2] and combined k and γ equations into one equation called k_γ. Although the approach of Sandhu and Ghosh [26] enables γ equation to be dropped, all functions in γ equation are included in the k equation. In addition, a cross-diffusion term is also added to the k equation. On the one hand, γ equation is disappeared, but on the other, it causes a pretty complex k equation to be solved.

Finally, Menter et al. [27] proposed an algebraic γ model. Although the model seems to have reduced-order nature and flexible structure, it introduces additional constants to provide a blending between calibrated values for low and high turbulence intensity. As a result, free coefficients are included in the model, so the similar problem seen in the γ-$\widetilde{Re_{\theta t}}$ model remained.

The primary motivation behind the present thesis is the question of whether the ideas of Bas et al. [20] could be applied in the $k-\omega$ SST turbulence model [28, 29]. Those ideas can be summarized as follows:

1. The turbulence model should be enough to transport the intermittency function. There should be no need for solving additional transport equation or equations. In other words, the turbulence model manipulated with an algebraic intermittency function should be sufficient to include transitional effects.

2. The intermittency function should be as simple as possible. The model should not be too complex and not have too many constants. Otherwise, a proper and safe calibration cannot be made as the experimental test cases are limited.

The SST turbulence model could be preferable in some types of problems, such as high-lift configurations, as it gives better results compared to the Spalart-Allmaras model [30]. The SST model is also desirable, where turbulence decay is important to be considered. SA-BCM model had some shortcomings, mainly due to the structure of the selected Spalart-Allmaras turbulence equation. Spalart-Allmaras model does not transport the turbulence kinetic energy itself but uses a working variable, $\widetilde{\nu}$, and relates it with the eddy viscosity. As a result, turbulence intensity decay through the domain is not calculated and cannot be provided to the correlation in the transition model. Therefore, the SA-BCM model assumes constant turbulence intensity, which causes the deviation of the predicted transition location from the actual one, especially in the presence of high freestream turbulent intensities, and limits the general applicability of the model [16].

In this thesis, a new transition model is proposed using a local correlation-based algebraic intermittency function. The γ_{BC} intermittency function of the SA-BCM model is taken as a baseline. This model is heavily modified without compromising its simplicity and coupled with the $k-\omega$ SST turbulence model to overcome the major shortcoming of the SA-BCM model, which is the lack of transportation of the turbulence intensity along the domain. The limitations in the SA-BCM model are eliminated without introducing any additional transport equation. This way, accurate results are obtained with much less computational cost compared with the models in the literature.

Chapter 2 of this thesis serves as a survey of the literature. The boundary layer transition mechanisms and the parameters affecting the transition are presented. The models used to predict the transition are given, and a discussion on some concepts is made at the end of this chapter. In Chapter 3, how the current transition model was developed is explained. After the complete formulation of the proposed model is presented, the calibration procedure is addressed. Chapter 4 summarizes validation studies and results obtained for experimental test cases. The present model is vali-

dated using ERCOFTAC T3 series flat plate cases [31], known as standard test cases for transition modeling, and also on some challenging 2D airfoil test cases. Finally, Chapter 5 concludes the thesis by evaluating the research outcomes and recommendations for future work.

CHAPTER 2

TRANSITION TO TURBULENCE

This chapter presents a literature survey on the transition to turbulence in boundary layer flows and its modeling. The first section describes the main transition modes, i.e., natural, bypass, and separation-induced, and the important parameters affecting the transition. In the second section of this chapter, the transition modeling methods are summarized with an explanation of their advantages and disadvantages. Lastly, some concepts encountered in transition modeling are discussed to provide a better understanding of the subject.

2.1 Transition Physics

2.1.1 Transition Modes

2.1.1.1 Natural Transition

Natural transition, or orderly transition, is the primary transition mode seen when the free-stream turbulence level is relatively low, less than 1% [15]. In Fig. 2.1, the schematic of the natural transition in a flow over a flat plate is given. The process starts with the appearance of two-dimensional Tollmien-Schlichting (T-S) waves in the streamwise direction. These instability waves gradually grow and break down after passing through a nonlinear stage, causing three-dimensional structures to form [32]. From this point, turbulent spots emerge [10]. As they expand and propagate downstream, the laminar portions disappear, and the flow becomes fully turbulent.

The point where the skin friction coefficient deviates from Blasius laminar profile is

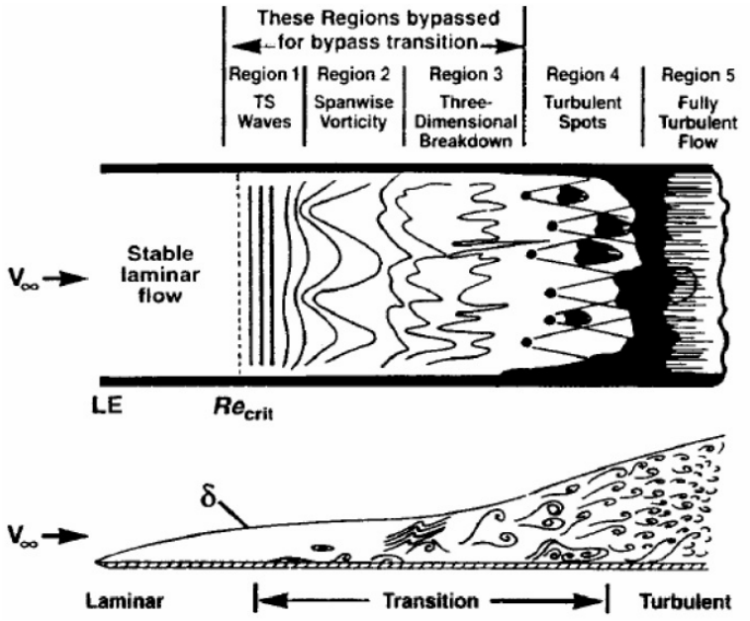

Figure 2.1: The natural transition process. Reproduced from Schlichting [33].

when the turbulent spots are formed [34]. Spots are intermittent turbulent portions, i.e., outside of them is still considered laminar while the spots encapsulate turbulent portions. A sketch and an experimental picture of turbulent spots are given in Fig. 2.2.

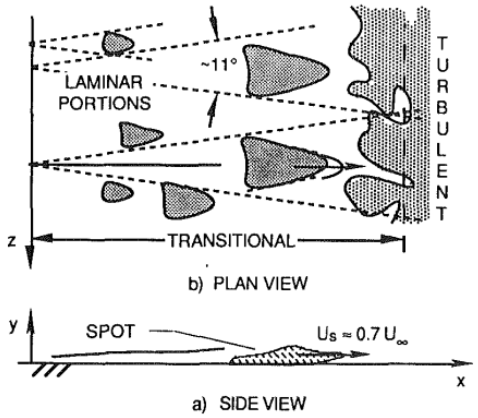

(a) Growth and propagation of turbulent spots. Reproduced from Mayle [15].

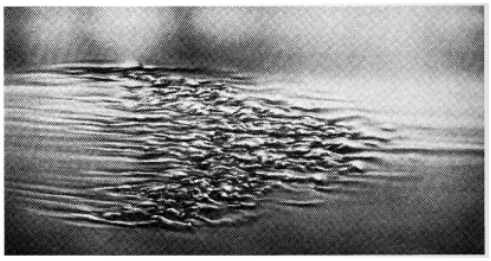

(b) Experimental picture of a turbulent spot. Reproduced from Schlichting [33].

Figure 2.2: Turbulent spot formation

2.1.1.2 Bypass Transition

The bypass transition is particularly relevant in cases where the flow has significant free-stream turbulence levels (higher than 1%) or when the boundary layer is subjected to high levels of external disturbances such as surface roughness, or incident wake flows [15]. Therefore, it is the main dominant mode seen in turbomachinery cases.

The term *bypass* comes from the fact that this mechanism bypasses the traditional natural instability route [35], where small perturbations grow and amplify through linear and nonlinear stages before leading to turbulence, as depicted in Fig. 2.1. As the formation and growth of T-S waves are not seen in this mechanism, it is not possible to make transition predictions using linear stability theory.

Measurements of Mayle and Schulz [36] showed that there is a significant level of unsteady velocity fluctuations in the pre-transitional flow field under the conditions of bypass transition. As a result of penetration of high amplitude disturbances, the laminar boundary layer is distorted, and jet-like streamwise elongated fluctuations, called *streaks* or *Klebanoff distortions*, are seen [18]. Those fluctuations grow downstream and cause a much faster breakdown than the natural transition mechanism. The turbulent spots are formed with the breakdown of the disturbances, and this point is where the significant deviation of skin friction coefficient from the laminar profile is seen, similar to natural transition.

A comparison of natural and bypass transition in terms of their effects on skin friction coefficient is depicted in Fig. 2.3, taken from Durbin [34]. Natural and bypass transition modes are pretty distinguishable from their pre-transitional behavior. The gradual growth of a regular oscillating instability wave, seen on the left pane of Fig. 2.3, indicates the natural way of transition. In contrast, the bypass route exhibits long wavelength and high amplitude pre-transitional fluctuations due to high levels of disturbances, seen on the right pane of Fig. 2.3.

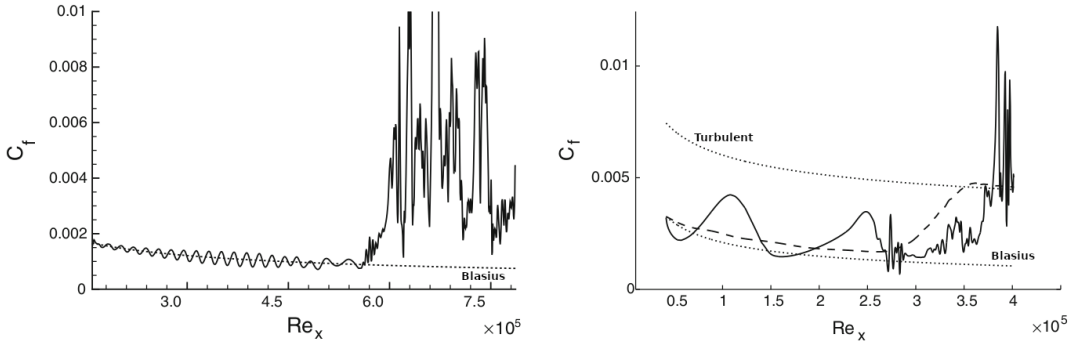

Figure 2.3: Left, skin friction beneath gradual growth of a regular oscillating instability wave. Right, skin friction fluctuations and bypass transition. Solid lines are instantaneous values, and the dashed line is time-averaged values. Reproduced from Durbin [34].

2.1.1.3 Separation-Induced Transition

Separation-induced transition is associated with *laminar separation bubbles (LSB)* formation. When a laminar flow is subjected to a strong adverse pressure gradient, the fluid particles having less momentum near the wall separate. The separated velocity profile is unstable due to its inflection point, and the transition may be triggered in the shear layer. Then, the turbulent flow may reattach due to enhanced momentum transfer. In this case, a reversed flow vortex is encapsulated in a region shaped like a bubble, which is called a *laminar separation bubble (LSB)* [15]. Within the bubble, the pressure stays constant until the transition onset. A representative sketch of the process is given in Fig. 2.4. In the figure, S denotes the point where laminar separation occurs, T indicates the transition onset point, and R is used where turbulent flow reattachs. The LSBs are commonly encountered on low Reynolds number airfoils whose Reynolds numbers vary between 10^4 and 10^6 [37].

2.1.2 Transition Parameters

The transition may be affected by many flow and geometric parameters. Broadly speaking, any factor affecting the laminar boundary layer has an influence on the transition [15]. However, the effect of some parameters, such as turbulence intensity,

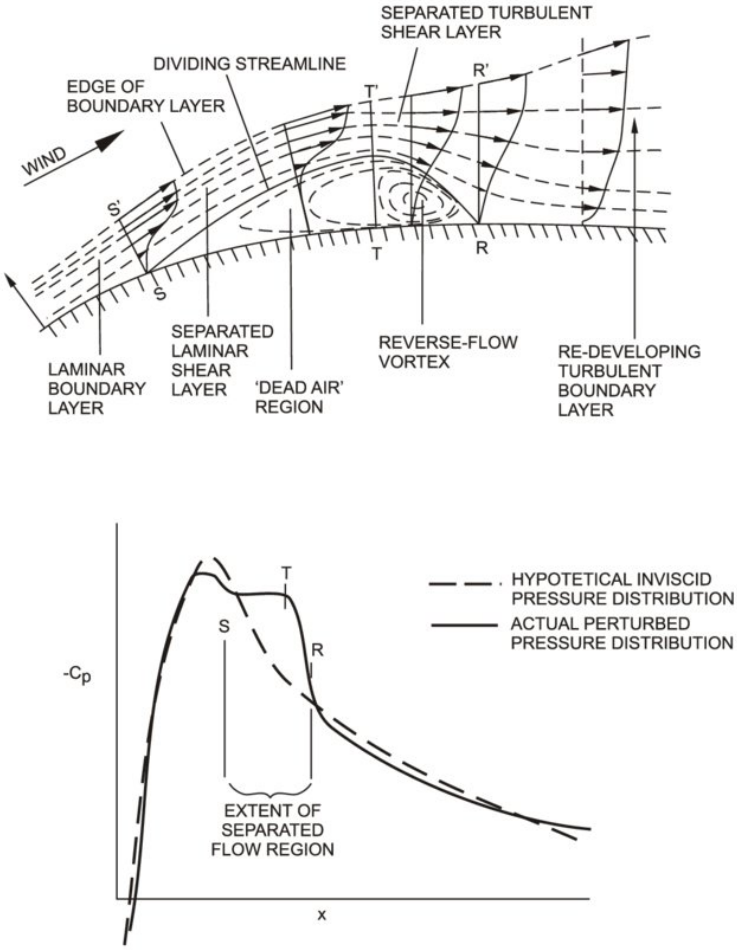

Figure 2.4: Sketch of a laminar separation bubble (top) and its effect on pressure coefficient (bottom). Adapted from Horton [38].

pressure gradient, and surface roughness, are more apparent and important than the others. Those affecting parameters are listed below.

2.1.2.1 Free-stream Turbulence Intensity

The free-stream turbulence intensity (Tu), defined as Eq. 2.1, is a measure of turbulence level in free-stream.

$$Tu = \frac{\sqrt{\frac{1}{3}\left(\overline{u'^2} + \overline{v'^2} + \overline{w'^2}\right)}}{U} = \frac{\sqrt{\frac{2}{3}k}}{U} \tag{2.1}$$

where $\overline{u'^2}$, $\overline{v'^2}$, $\overline{w'^2}$ are normal Reynolds stress components, k is turbulent kinetic energy, and U is free-stream mean flow velocity.

The free-stream turbulence intensity is the most influential parameter for the transition. The experimental correlations used to predict the transition onset, e.g., the one of Abu-Ghannam and Shaw [14], are strong functions of turbulence intensity. As the turbulence intensity increase, the Reynolds number at which the transition begins reduces. High levels of free-stream turbulence intensity are signals for bypass transition.

2.1.2.2 Pressure Gradient

The effect of the pressure gradient is only significant when the free-stream turbulence intensity is relatively low [15]. Its effect can be neglected in the presence of high Tu values, and in fact, that is what is done in the correlation of Mayle [15], which is only a function of free-stream turbulence intensity. When the laminar flow is subjected to an adverse pressure gradient, the transition point is shifted upstream due to the destabilization of the boundary layer. Conversely, the favorable pressure gradient delays the transition onset.

2.1.2.3 Surface Roughness

Surface roughness causes disturbances in the boundary layer flow, and as a result, the transition process is shifted upstream. However, three-dimensional surface roughnesses sometimes may be exploited to delay the transition [39], so the transition control is possible by means of surface roughness.

2.2 Transition Prediction

As depicted in the previous section, the transition has distinct mechanisms through turbulence, and there is no unified theory. Therefore, the transition prediction efforts mostly rely on modeling. Although simulation methods, DNS and LES, stand as

appealing alternatives, their demand for computational power is still so huge that their use in practical engineering purposes is highly limited [40]. Thus, they are excluded here.

Various models have been proposed over the years, and some of them are more successful in some types of flows, while others show their advantage in different types of flow conditions. A precise categorization of all of these models may not be possible as some models combine different features that belong to separate modeling concepts. In this section, only a basic framework is drawn, and a brief selective review of those modeling concepts is given.

2.2.1 e^N Method

One of the oldest and most mature methods to predict the transition is the e^N method [4, 3] based on the traction of growth of disturbance amplitudes within the boundary layer flow. e^N method does not provide flow field solutions in contrast to RANS-type transition models, but it is just a transition indication method.

This method needs the calculation of the laminar flow field to have laminar velocity and temperature profiles along the body. Then, the local amplification rate of unstable waves is computed using local stability equations, and the local rate is integrated along a streamline. As a result of this integration process, a global amplification factor *N* showing the ratio of growth of disturbances from their initial amplitude to a given streamwise position is obtained. Once the global amplification factor exceeds a critical value, the transition process begins.

The main problem with the e^N method is its inability to account for the transition caused by nonlinear effects because it is based on linear stability theory. Therefore, it is only suitable for the prediction of natural transition. In addition, the selection of the *N* factor is not universal and needs experimental correlations to be generalized [41], so e^N is accepted as a semi-empirical method.

The common way to utilize the e^N method is the coupling with boundary-layer codes since typical Navier-Stokes solvers do not provide enough accuracy for the flow field to evaluate the stability equations that the method needs [42]. Although it is quite

complicated and requires complex infrastructure, the utilization of the e^N method coupled with RANS approaches is possible for specialized purposes [43, 44, 45].

Recently, a novel approach to mimic the methodology of the e^N method in a local RANS-type formulation has been adopted in Amplification Factor Transport (AFT) model by Coder and Maughmer [46]. They eliminated the calculation of the integral parameters by suggesting a simplified non-dimensional pressure gradient parameter. Then, they derived a transport equation for an amplification factor, $\tilde{n}$, based on the simplified linear stability theory to track the growth of Tollmien-Schlichting waves. The factor is used to trip the turbulence model once it exceeds the critical N-factor, similar to the original e^N method.

2.2.2 Low Reynolds Number Turbulence Models

The first inherently RANS-type transition prediction method was the use of a low Reynolds number turbulence model. Low Reynolds number turbulence models were initially intended to support laminar regions where the local Reynolds number is dropped. For instance, the very near the wall is always laminar due to the formation of a viscous sublayer. As turbulence models were derived by making the fully turbulent assumption, the utilization of wall functions was essential to solve boundary layer flows. Low Reynolds number turbulence models, first proposed by Jones and Launder [9], use wall damping functions to eliminate this need. Although they did not specifically aim to model the transition, their ability to predict the bypass transition was seen to some extent. This was because of the similarities in the behavior of the viscous sublayer and developing laminar boundary layer [47]. Zheng et al. [48] showed that low Reynolds number models predict too early onset of the transition and do not have enough sensitivity to separation-induced transition if any further modifications are not performed.

Various low Reynolds number turbulence models that are specifically devoted to predicting transition were also proposed. Some of them are the one of Wilcox [49] and the one of Langtry and Sjolander [50]. Although these formulations enable some improvement, the transition calibration has an interaction between their viscous sublayer formulation. Therefore, they suffer from calibration issues [5]. In addition,

low Reynolds number turbulence models mostly suffer from robustness and accuracy problems [42], so the reliability of the results that they offer is questionable.

2.2.3 Laminar Kinetic Energy (LKE) Models

These models are based on the estimation of the laminar fluctuations seen in the pre-transitional boundary layer when the free-stream turbulence intensity is sufficiently high to make the transition mode bypass type. Those laminar fluctuations have high amplitude and are distinguishable from turbulent fluctuations. Mayle and Schulz [36] introduced the idea of solving another kinetic energy equation to estimate these laminar fluctuations, similar to the transport equation for turbulent kinetic energy, and named the equation as laminar kinetic energy equation. The source terms of their model needed non-local information. Walters and Leylek [51] introduced a fully local formulation in their three equation k_L-k_T-ϵ model, and later, Walters and Cokljat [52] proposed the k_L-k_T-ω model, an improved version of the previous model.

In simple terms, the models based on laminar kinetic energy initiate the transition once the fluctuations reach a critical level. They generally involve three transport equations, but four equation variations also exist, e.g., the model of Pacciani et al. [53]. A recent interesting model is the algebraic model of Kubacki and Dick [54]. They derived an algebraic transition model for turbomachinery applications combining the laminar kinetic energy concept with an intermittency function and coupled it with the $k-\omega$ turbulence model [55]. Although it can be considered as a combined model, the main rationale still relies on the division of fluctuations to express eddy viscosity as a sum of small-scale and large-scale eddy viscosity. Later, an extended version of this model to improve the prediction of separation-induced transition was proposed by Kubacki et al. [56].

2.2.4 Intermittency Models

Intermittency models introduce the *intermittency* concept to the model equations. The basic idea is to provide a probability distribution for turbulence by using an *intermittency factor,* γ, that is zero in the laminar flow regime and converges to one when the

flow turns turbulent. A formulation for this factor was first proposed to describe the formation of turbulent spots by Emmons [10] and further improved by Dhawan and Narasimha [11] using a wide range of experiments. Dhawan and Narasimha [11] suggested a generalized intermittency function related to turbulent spot production and transition location. The algebraic intermittency function of Dhawan and Narasimha [11], given in Eq. 2.2, is appealing because of its simplicity and ability to represent the intermittency distribution depending on turbulence parameters.

$$\gamma = \begin{cases} 1 - exp\left(-\frac{(x - x_t)^2 n\sigma}{U}\right) & (x \geqslant x_t) \\ 0 & (x < x_t) \end{cases} \tag{2.2}$$

where x is the streamwise position, x_t is the transition onset point, n is the formation rate of the turbulent spots, σ is the propagation rate of the turbulent spots, and U is the free-stream velocity.

Later, Steelant and Dick [12] and, following, Suzen and Huang [13] developed a transport equation for intermittency to reproduce the intermittency profile of Dhawan and Narasimha [11]. They also coupled this intermittency equation with two-equation turbulence models to manipulate turbulence production.

As the intermittency formulation depends on transition location, x_t, to be known, these models search x_t throughout the domain by calculating *momentum thickness Reynolds number,* Re_θ, which is the sign of transition location once it exceeds a critical value ($Re_\theta \geqslant Re_{\theta t}$) as in the e^N method. Therefore, two parameters, i.e., *local momentum thickness Reynolds number* Re_θ and *transition momentum thickness Reynolds number* $Re_{\theta t}$, become essential to evaluate intermittency, which both require *non-local information*. Momentum thickness Reynolds number Re_θ is defined as in Eq. 2.3.

$$Re_\theta = \frac{\rho_\infty U_\infty \theta}{\mu_\infty} \tag{2.3}$$

θ is the momentum thickness and is given in equation 2.4.

$$\theta = \int_0^\infty \frac{\rho}{\rho_\infty} \frac{u}{U_\infty} \left(1 - \frac{u}{U_\infty}\right) dy \tag{2.4}$$

In the last two equations, ρ is the density, μ is the dynamic viscosity, u is the local velocity, and ∞ subscript is used for free-stream values. By definition, taking integrals normal to the walls is necessary to pursue local momentum thickness Reynolds number Re_θ through the domain, and those integrals might even be impossible to evaluate on the complex shaped geometries or on the domains using unstructured meshes [6, 8]. As for transition momentum thickness Reynolds number $Re_{\theta t}$, it is calculated using experimental correlations like that of Mayle [15]. Because those correlations depend on free-stream turbulence intensity, relevant non-local data has to be provided to the computational cells inside the boundary layer. The main difficulty in correlation-based methods stems from calculating those two parameters.

To overcome issues related to non-local parameters, Menter et al. [6] proposed a novel approach suggesting to use of a local parameter called *vorticity Reynolds number* Re_v, introduced by van Driest and Blummer [17], instead of direct calculation of Re_θ. Menter et al. argued [5] maximum point of Re_v through the boundary layer is proportional to local Re_θ with an acceptable error. Thus, the relation in Eq. 2.3 is replaced with Eq. 2.5. In Appendix A, a more detailed explanation and a derivation for this replacement are given.

$$Re_\theta = \frac{\max\left(Re_v\right)}{2.193} \tag{2.5}$$

where

$$Re_v = \frac{\rho d_w^2}{\mu} \Omega \tag{2.6}$$

In Eq. 2.6, ρ is the density, μ is the dynamic viscosity, Ω is the magnitude of the vorticity rate, and d_w is the minimum wall distance.

As mentioned earlier, the other issue was the need for non-local information for the correlations to detect the transition onset. In the early one-equation γ model of Menter et al. [6], the transition onset criterion was provided through a constant user-defined

critical Reynolds number. This model was subsequently used as a baseline for the γ-$\widetilde{Re_{\theta t}}$ model of Langtry and Menter [8, 5, 7]. In this model, another transport equation for $\widetilde{Re_{\theta t}}$ was added to calculate the transition onset correlation locally. Thus, this new model became the first correlation-based transition model based on an entirely local formulation. Menter et al. [7] called this model framework *Local Correlation-Based Transition Modeling (LCTM)*. The γ-$\widetilde{Re_{\theta t}}$ model is validated by different research groups [18] and has shown its success in general applications [19]. In addition, various modifications have been introduced to the γ-$\widetilde{Re_{\theta t}}$ model of Menter et al. [5] to improve the model, such as the inclusion of the cross-flow instability effects by Seyfert and Krumbein [57], Medida and Baeder [58], Grabe and Krumbein [59] and also by Langtry [60], the inclusion of surface roughness effects by Dassler et al. [61], and the inclusion of compressibility effects Kaynak [62].

The model of Lodefier et al. [63] is also one of the early intermittency models. The model uses vorticity Reynolds number Re_v as Re_θ, which makes the model very similar to early γ model of Menter et al. [6], but Lodefier et al. [63] use the correlation of Mayle [15] for transition onset unlike the early γ model of Menter et al. [6] which needs constant critical value to be defined. Production term in the model of Lodefier et al. [63] is based on that of Steelant and Dick [12]. Later, Lodefier and Dick [64] modified this model to support unsteady simulations and separated intermittency into two equations for near and free-stream intermittency.

Some intermittency-based models have also been derived without external experimental correlations. These models detect the transition using some carefully calibrated threshold functions. An example of these models is the one-equation intermittency model proposed by Ge et al. [65], which is an improved version of [66]. Their model is capable of predicting bypass and separation-induced transition. A recent example is the one-equation γ model of Juntasaro et al. [67]. This model makes use of only one sensing function for both natural and bypass transition, and separation is predicted using the same function previously proposed by Ge et al. [65].

Although some success has been achieved in predicting the transition, the main drawback of the aforementioned models is their need for significantly more computational power than standard turbulence models, as they all require solving at least one ad-

ditional transport equation. This is even worse for the γ-$\widetilde{Re_{\theta t}}$ model as it needs yet another transport equation for $\widetilde{Re_{\theta t}}$.

Baş et al. [20] proposed a very straightforward algebraic intermittency model. Their model makes use of the correlation of Menter et al. [5] to detect the transition onset point by checking the vorticity Reynolds number, Re_v, and releases the underlying turbulence model when the transition is completed. They manipulated only the production term of the Spalart-Allmaras turbulence model [21] with the inclusion of their intermittency function. The combined model is called the SA-BC transition model [20, 16], and later with further improvements, the SA-BCM model [22, 23]. The SA-BC model showed good results compared to higher order transition models can be obtained using only turbulence equation [24].

Meanwhile, the γ-$\widetilde{Re_{\theta t}}$ model followed its simplification path. Coder and Maughmer [25] tried to simplify the γ-$\widetilde{Re_{\theta t}}$ model by means of a correlation based on a non-dimensional local pressure-gradient parameter. Later, Menter et al. [2] proposed the γ model as a simplification of the γ-$\widetilde{Re_{\theta t}}$ model by dropping $\widetilde{Re_{\theta t}}$ equation and adjusting the functions and coefficients. They suggested local turbulence intensity and pressure gradient formulations to avoid the use of free-stream values in the onset correlation. A sophisticated modification was performed by Sandhu and Ghosh [26] to simplify γ model [2] combining k and γ equations into one equation called k_γ. Finally, Menter et al. [27] proposed an algebraic γ model. The prominent feature of this model is the blending of the model constants between calibrated values for low and high turbulence intensity.

2.3 On Some Concepts in Transition Modeling

2.3.1 Locality

Locality is a notion that widely came across in transition modeling, so it would be beneficial to explain it. Locality is associated with the available information inside each computational cell. The parameters known or possible to be computed using only present information inside a cell are *local*. So a local formulation necessitates

that the information transfer can only be between adjacent cells through fluxes in the context of the finite volume scheme. In order words, any information transfer from non-adjacent cells is a *non-local operation*.

Locality gains importance in modern general-purpose CFD codes, whose grid data structures are based on unstructured format and parallel execution is a daily routine [8], as a non-local operation like taking integral generally requires additional search and integration algorithms [16]. Even though it is possible to build the essential infrastructure, particularly in special-purpose codes, non-local operations significantly increase the computational burden. Therefore, the local formulation is a quite desirable feature for modern models.

2.3.2 Turbulence Intensity

As explained in previous sections, turbulence intensity is the primary parameter in the correlations. However, there exists some ambiguity about the turbulence intensity term in the correlations, and it constitutes a source of error. The term of *free-stream turbulence intensity (FSTI)* is not that clear to use a correlation safely because each correlation may have its own free-stream definition [68]. For example, the correlation of Abu-Ghannam and Shaw [14] makes use of an average value taken halfway the leading edge and the transition onset location. Similarly, in the correlation of Mayle [15], the same method is thought to be followed though it is not explicitly remarked [18]. On the other hand, the correlation of Suzen and Huang [13] employs FSTI at the transition onset location. As for the initial correlation of Menter et al. [5], it is obtained by fitting a new curve to the correlations in question and experimental data collected by different groups and gets use of local FSTI in the implementation. The correlation of Langtry and Menter [8], which is an improved version of that proposed by Menter et al. [5] to predict natural transition better, uses local FSTI, too.

The transition onset location may also be different than that found using correlations due to the length scale effects [69]. Dick and Kubacki [18] indicate using a halfway location (between the leading edge and the transition onset) to evaluate FSTI enables to improve predictions (as can be expected); however, there may still be some gap between the transition location and the predictions especially when large length scales

dominate. They also point out that the use of FSTI at transition onset location will probably result in predicting the onset too late, and finally, they suggest that the correlation by Langtry and Menter [8] is the most reliable correlation.

CHAPTER 3

DEVELOPMENT OF THE MODEL

This chapter describes the fundamentals of the model proposed in the current thesis work. As the proposed model relies on the ideas of the SA-BCM model, an introduction and formulation for the SA-BCM model is given. Model formulation and the process of development of the model are presented. The last section explains how the calibration tasks are performed.

3.1 SA-BCM Model

Bas-Cakmakcioglu (BC) model is an algebraic intermittency-based transition model proposed by Bas et al. [20]. The model is coupled with the Spalart-Allmaras (SA) turbulence model [21], and only interaction with the turbulence model is by means of the manipulation of the production term. The main rationale in the SA-BC model is that a well-defined correlation-based intermittency function would be enough to control the turbulence model and it is an unnecessary task to set up an equation only for the transportation of the intermittency through the domain. Starting from this point, they proposed an intermittency function γ_{BC} which is defined in Eq. 3.1.

$$\gamma_{BC} = 1 - e^{-\left(\sqrt{Term1}+\sqrt{Term2}\right)} \tag{3.1}$$

$Term1$ in Eq. 3.1 is defined in Eq. 3.2. Physically, it is the term responsible for triggering the transition. Once the momentum thickness Reynolds number, Re_θ, exceeds a critical value provided by $Re_{\theta c}$ correlation, the transition process is initiated and γ_{BC} starts to grow.

$$Term_1 = \frac{max(Re_\theta - Re_{\theta c}, 0.0)}{\chi_1 Re_{\theta c}} \tag{3.2}$$

where Re_θ given in Eq. 3.3 is calculated using vorticity Reynolds number, Re_v, as suggested by Menter et al. [5].

$$Re_\theta = \frac{\max(Re_v)}{2.193} \tag{3.3}$$

where Re_v is defined in Eq. 3.4.

$$Re_v = \frac{\rho d_w^2}{\mu}\Omega \tag{3.4}$$

Here, ρ stands for density, d_w is minimum wall distance, μ is dynamic viscosity, and Ω represents the magnitude of the vorticity.

Critical momentum thickness Reynolds number, $Re_{\theta c}$, is calculated based on the correlation of Menter et al. [5].

$$Re_{\theta c} = 803.73\,(Tu_\infty + 0.6067)^{-1.027}$$

where Tu_∞ is the free-stream turbulence intensity in percent, and it is assumed as constant.

$Term2$ in Eq. 3.1 is defined in Eq. 3.5. It is responsible for activating γ_{BC} near-wall regions. The purpose of $Term2$ in the model is not for triggering but for supporting the transition process.

$$Term_2 = \frac{max(\nu_{BC} - \chi_2), 0.0}{\chi_2} \tag{3.5}$$

where

$$\nu_{BC} = \frac{\nu_t}{U d_w} \tag{3.6}$$

where ν_t is turbulent viscosity, U is local velocity magnitude, and d_w is minimum wall distance.

As $Term2$ included an explicit appearance of local velocity magnitude, it violated the Galilean-invariance principle. Even though it does not pose a big problem if the reference frame is fixed and the domain does not have any moving walls, the Galilean-invariance is a desirable feature for any model. Then, the model developers [22] improved the model and suggested a new $Term2$ formulation satisfying the Galilean-invariance. The improved model is called SA-BCM (Spalart-Allmaras Bas-Cakmakcioglu with Modifications), and the latest $Term2$ formulation is given in Eq. 3.7.

$$Term_2 = \max\left(\frac{\mu_t}{\chi_2 \mu}, 0.0\right) \tag{3.7}$$

where μ_t is turbulent eddy viscosity, and μ is the dynamic viscosity.

The model constants χ_1 in Eq. 3.2 and χ_2 in Eq. 3.7 are 0.002 and 0.02, respectively.

Finally, the model is coupled with the SA turbulence model as in Eq. 3.8. The only difference in the original model equation is the inclusion of the γ_{BC} into the production term.

$$\frac{\partial \tilde{\nu}}{\partial t} + u_j \frac{\partial \tilde{\nu}}{\partial x_j} = \tilde{P}_{\tilde{\nu}} - D_{\tilde{\nu}} + \frac{1}{\sigma}\left[\frac{\partial}{\partial x_j}\left((\nu + \tilde{\nu})\frac{\partial \tilde{\nu}}{\partial x_j}\right) + c_{b2}\frac{\partial \tilde{\nu}}{\partial x_j}\frac{\partial \tilde{\nu}}{\partial x_j}\right] \tag{3.8}$$

where

$$\tilde{P}_{\tilde{\nu}} = \gamma_{\mathbf{BC}} P_{\tilde{\nu}} \tag{3.9}$$

where $P_{\tilde{\nu}}$ is the original production term of the SA model. All other details of the SA model can be found in Ref. [21].

3.2 Proposed Formulation

The current algebraic model carries the same spirit as the SA-BC model [20], and uses an intermittency function ϕ to manipulate the source terms of the underlying turbulence model to capture transition behavior. ϕ function enables damping turbulence kinetic energy production until the transition onset criterion is met and converges to $\phi = 1$ to release the underlying turbulence model when the transition to turbulence is completed.

The intermittency function ϕ of the present model preserves the same form used in the SA-BC model [16] as given in Eq. 3.10. Basically, the intermittency function ϕ consists of two terms, i.e., one term to control the transition onset utilizing the correlation, and a second term to enable the diffusion of the intermittency near the wall.

$$\phi = 1 - e^{-(Term1+Term2)} \tag{3.10}$$

$Term1$ given in Eq. 3.11 is responsible for triggering the transition onset based on the correlation. It has the same formulation as SA-BCM [22]; however, the critical momentum thickness Reynolds number $Re_{\theta c}$ correlation is modified to use the local turbulence intensity definition suggested by Menter et al. [2].

$$Term1 = C_1 \left[\max \left(\frac{Re_\theta}{Re_{\theta c}} - 1,\ 0 \right) \right]^{0.5} \tag{3.11}$$

Re_θ definition given in Eq. 3.12 is again calculated based on Re_v proportionality, and the constant 2.193 is not changed.

$$Re_\theta = \frac{\max\left(Re_v\right)}{2.193} = \frac{\rho d_w^2\, \Omega}{2.193\, \mu} \tag{3.12}$$

where ρ is the density, μ is the dynamic viscosity, Ω is the magnitude of the vorticity, and d_w is the minimum wall distance.

Because the SA-BCM is ultimately based on the Spalart-Allmaras turbulence model, the turbulence kinetic energy k is not calculated, and turbulence intensity decay through the domain cannot be known. Therefore, the transition onset correlation in the SA-BCM model has to make use of a constant turbulence intensity assump-

tion, which limits its generality as the turbulence intensity may experience significant changes through the domain. The use of the SST model enabling the direct calculation of turbulence intensity overcomes this deficiency. However, another issue appears: A nonlocal information transfer is needed between the computational cells since the transition correlations are based on free-stream turbulence intensity. In addition, the Galilean-invariance principle is violated because the turbulence intensity definition depends on the velocity. Menter et al. [2], as a remedy, proposed a local turbulence intensity formulation given in Eq. 3.13 that provides a reasonable estimation for free-stream turbulence intensity.

$$Tu_L = \max\left(100\frac{\sqrt{2k/3}}{\omega d_w}, 100\right) \tag{3.13}$$

Menter et al. [2] proposed a simplified fully local $Re_{\theta c}$ correlation, given in Eq. 3.14, using this new turbulence intensity definition. In the present model, the correlation of Menter et al. [2] is preferred to make the model locally formulated. As that enables a simple way of fully local formulation in a two-equation k-ω SST framework, given the issues mentioned above.

$$Re_{\theta c} = 100.0 + 1000.0\exp(-Tu_L F_{PG}) \tag{3.14}$$

This $Re_{\theta c}$ correlation includes a pressure gradient correction term, Eq. 3.15, which is also locally calculated.

$$F_{PG} = \begin{cases} \min\left(1 + 14.68\lambda_{\theta L}, 1.5\right) & \lambda_{\theta L} \geq 0 \\ \min\left(1 - 7.34\lambda_{\theta L}, 3.0\right) & \lambda_{\theta L} < 0 \end{cases} \tag{3.15}$$

Here, the pressure gradient parameter is calculated as follows.

$$\lambda_{\theta L} = -7.57 \cdot 10^{-3}\frac{dV}{dy}\frac{d_w^2}{\nu} + 0.0128 \tag{3.16}$$

$$\frac{dV}{dy} = \nabla\left(\overrightarrow{n} \cdot \overrightarrow{V}\right) \cdot \overrightarrow{n} \tag{3.17}$$

$$\overrightarrow{n} = \frac{\nabla(d_w)}{|\nabla(d_w)|} \tag{3.18}$$

$Term1$ alone cannot enable the diffusion of the intermittency function ϕ into the depth of the boundary layer because it converges to very low values close to the wall due to its dependence on wall distance seen in Eq. 3.12. Another term, $Term2$, is needed to complete the model for that purpose. $Term2$ is again similar to SA-BCM [22] such that both use turbulent Reynolds number Re_T, viscosity ratio. However, the structure of $k-\omega$ based models leads us to use a different function than that in SA-BCM [22]. Direct use of old formulation induces $Term2$ to be activated everywhere in the domain; therefore, $Term2$ is adjusted to increase more slowly at low turbulent Reynolds numbers Re_T. The new proposed $Term2$ is given in Eq. 3.19.

$$Term2 = C_2 \left(Re_T\right)^{3.5} \tag{3.19}$$

Here, turbulent Reynolds number Re_T is calculated as in Eq. 3.20.

$$Re_T = \frac{\rho k}{\omega \mu} \tag{3.20}$$

where ρ is the density, and μ is the dynamic viscosity.

It should also be noted that the current formulation of $Term2$ has another impact on the model. As the destruction term of the k equation in Eq. 3.40 is limited depending on the value the intermittency function ϕ takes, there exists a risk that freestream turbulence intensity decay may be distorted if the intermittency function ϕ is not completely turned on at the freestream. Therefore, $Term2$ also ensures the intermittency function is active at the freestream.

In the present model, a separation correction term is proposed to improve the behavior of the underlying turbulence model in case of separation. Since the transition model eventually relies on the turbulence model used to predict the turbulent flow, it inherits the shortcomings of the turbulence model. It is known that turbulence kinetic energy (k) production of the SST model is insufficient to reattach the flow at the correct location for separation-induced transition [5, 2]. Preliminary results showed that the turbulent reattachment location is consistently found downstream unless a correction term is utilized. The correction method preferred in the current model is to allow the intermittency function ϕ to exceed one such that the turbulence production is exaggerated to generate the required turbulence kinetic energy k rapidly. The proposed

separation function ϕ_{sep} given in Eq. 3.21 has a simpler formulation compared to the separation correction functions of other models [5, 2, 67, 65, 56] in the literature. It basically consists of two controllers, F_{on} and F_{off}, i.e., one for activation of the correction term and one for turning it off.

$$\phi_{sep} = \min\left(F_{on}F_{off}, C_{sep}\right) \tag{3.21}$$

Here, similar to the approach of Langtry and Menter [8], F_{on} function is simply based on the ratio of the vorticity Reynolds number Re_v to the critical momentum thickness Reynolds number $Re_{\theta c}$. Similarly, the scaling coefficient is set to 3.235, which provides the shape factor (H) at the separation point. F_{off} checks whether $Term2$ is turned on, and if so, it turns off the correction term. C_{sep} controls how strongly the separation correction is effective, as the larger C_{sep},the smaller the separation bubble size. The separation correction term is kept as straightforward as possible and relies on the functions that have already been calculated.

$$F_{on} = \max\left(\left(\frac{Re_v}{3.235Re_{\theta c}}\right) - 1, 0\right) \tag{3.22}$$

$$F_{off} = \max\left(1 - Term2, 0\right) \tag{3.23}$$

Then, the effective intermittency function ϕ_{eff} used to manipulate the production term of k equation in Eq. 3.27 is calculated as in Eq. 3.24.

$$\phi_{eff} = \max\left(\phi, \phi_{sep}\right) \tag{3.24}$$

Finally, the model constants are given as follows.

$$C_1 = 2000, \quad C_2 = 0.1, \quad C_{sep} = 2.7 \tag{3.25}$$

3.2.1 Coupling with SST k-ω Turbulence Model

The present transition model is coupled with the Shear Stress Transport (SST) turbulence model of Menter [28] as given in Eq. (3.26) and (3.27).

$$\rho\frac{Dk}{Dt} = \tilde{P}_k - \tilde{D}_k + \frac{\partial}{\partial x_j}\Big[(\mu + \mu_t\sigma_k)\frac{\partial k}{\partial x_j}\Big] \tag{3.26}$$

$$\rho\frac{D\omega}{Dt} = \frac{\alpha}{\nu_t}P_k - D_w + \frac{\partial}{\partial x_j}\Big[(\mu + \mu_t\sigma_\omega)\frac{\partial \omega}{\partial x_j}\Big] + CD_w \tag{3.27}$$

where P_k, D_k and CD_w are production, destruction and cross-diffusion terms of the original SST turbulence model, respectively. Those are defined as follows in Eq. 3.28, 3.29, and 3.30.

$$P_k = \min\left(\mu_t S^2, 10 D_k\right) \tag{3.28}$$

$$D_k = \beta^* \rho \omega k \tag{3.29}$$

$$CD_w = 2\left(1 - F_1\right) \frac{\rho \sigma_{\omega 2}}{\omega} \frac{\partial k}{\partial x_j} \frac{\partial \omega}{\partial x_j} \tag{3.30}$$

The turbulent eddy viscosity is computed as in Eq. 3.31.

$$\mu_t = \min\left[\frac{\rho k}{\omega}, \frac{a_1 \rho k}{S F_2}\right] \tag{3.31}$$

The blending functions F_1 and F_2 are defined in Eq. 3.32 and 3.35.

$$F_1 = \tanh\left(\arg_1^4\right) \tag{3.32}$$

$$\arg_1 = \min\left[\max\left(\frac{\sqrt{k}}{\beta^* \omega d}, \frac{500\nu}{d^2 \omega}\right), \frac{4\rho \sigma_{\omega 2} k}{\mathrm{CD}_{k\omega} d^2}\right] \tag{3.33}$$

$$\mathrm{CD}_{k\omega} = \max\left(2\rho \sigma_{\omega 2} \frac{1}{\omega} \frac{\partial k}{\partial x_j} \frac{\partial \omega}{\partial x_j}, 10^{-10}\right) \tag{3.34}$$

$$F_2 = \tanh\left(\arg_2^2\right) \tag{3.35}$$

$$\arg_2 = \max\left(2\frac{\sqrt{k}}{\beta^* \omega d}, \frac{500\nu}{d^2 \omega}\right) \tag{3.36}$$

Each constant in the SST model is blended between k-ω and k-ϵ regions using the function in Eq. 3.37.

$$\varphi = F_1 \varphi_1 + \left(1 - F_1\right) \varphi_2 \tag{3.37}$$

Here, φ_1 represents the constant values in inner k-ω region, and φ_2 is for values in outer k-ϵ region. The model constants are as follows.

$$\alpha_1 = 5/9, \quad \alpha_2 = 0.44,$$

$$\begin{aligned} \sigma_{k1} = 0.85, \quad \sigma_{\omega 1} = 0.5, \quad \beta_1 = 0.075, \\ \sigma_{k2} = 1.0, \quad \sigma_{\omega 2} = 0.856, \quad \beta_2 = 0.0828, \\ \beta^* = 0.09, \quad \kappa = 0.41, \quad a_1 = 0.31 \end{aligned}$$

Note that some of the model constants above are corrected according to Menter et al. [29], and for production term P_k, Kato-Launder correction [70] given in Eq. 3.38 is used instead of the original P_k in Eq. 3.28.

$$P_k = \mu_t S \Omega \tag{3.38}$$

where Ω is the magnitude of the vorticity rate, and S is the magnitude of the strain rate.

Modified production and destruction terms of the turbulent kinetic energy equation are given in Eq. (3.39) and (3.40).

$$\tilde{P_k} = \phi_{eff} P_k \tag{3.39}$$

$$\tilde{D_k} = max(\phi, 0.1) D_k \tag{3.40}$$

The intermittency function ϕ should also be limited not to drop below the factor of $C_3 = 1/20$ as explained in the model calibration section. This can simply be performed using max function as follows.

$$\phi = \max(\phi, C_3) \tag{3.41}$$

The modification of F_1 blending function in the SST model is also used to avoid any issues related to the switch between k-ω to k-ϵ model near the wall, as suggested by Menter et al. [5].

$$R_y = \frac{\rho y \sqrt{k}}{\mu}, \quad F_3 = \exp\left(-\frac{R_y}{120}\right)^8, \quad F_1 = \max\left(F_{1orig}, F_3\right) \tag{3.42}$$

where F_{1orig} is the original blending function of the SST model.

3.2.2 Assessment of Limiters on Turbulence Terms

The model includes two essential limiters. The obvious limiter applied on the destruction term of the turbulence kinetic energy equation given in Eq. 3.40 appears in several models [5, 2, 67]. However, the mentioned studies do not provide the theory and reasoning for this limiter.

The importance of the other limiter, i.e., the lower limiter for intermittency function ϕ in Eq. 3.41, may not immediately be recognized because the intermittency is generally bounded at its transport equation using a constant coefficient in the equation. Hence, the approach that these models adopt may be considered as an implicit limiter. Since we eliminate the intermittency equation, the intermittency should be controlled by a limiter.

Therefore, it can be said that there is a common base leading the model makers to preserve the same limiter form, although the transition models look different. Revealing the effects of these limiters on any model would be guiding for the other models that will benefit from them.

3.2.2.1 Destruction Term Limiter

By *the destruction term limiter,* it is meant *the limiter in the destruction term of turbulence kinetic energy equation*. As seen in Eq. 3.40, the destruction term is controlled depending on the value that the intermittency function takes, not the actual value of the destruction term. Therefore, one should be careful not to be confused by the terminology.

Although this limiter seems one of the inevitable ingredients for intermittency models coupled with two-equation turbulence models, given its inclusion in various models

[5, 2, 26, 67], its justification had not been addressed until some recent works have shed light on the use of this limiter.

Sandhu and Ghosh [71] investigated the behavior of their algebraic k_γ model [26], which is a simplified model derived from γ model of Menter et al. [2]. They performed a dynamical system analysis and concluded that the destruction term limiter enables the model to provide a stable solution for the laminar region. The paper of Coder and Maughmer [30] also presents valuable clues about the near-wall behavior of transition models based on the SST turbulence model. They showed that the destruction term limiter corrects the log-layer behavior of $\gamma - Re_\theta$ model as represented in Fig. 3.1 though some scaling errors come with it. They gradually increased the destruction term lower limiter and found a value of 0.1, which is the published value by Menter et al. [5], enabling proper offset.

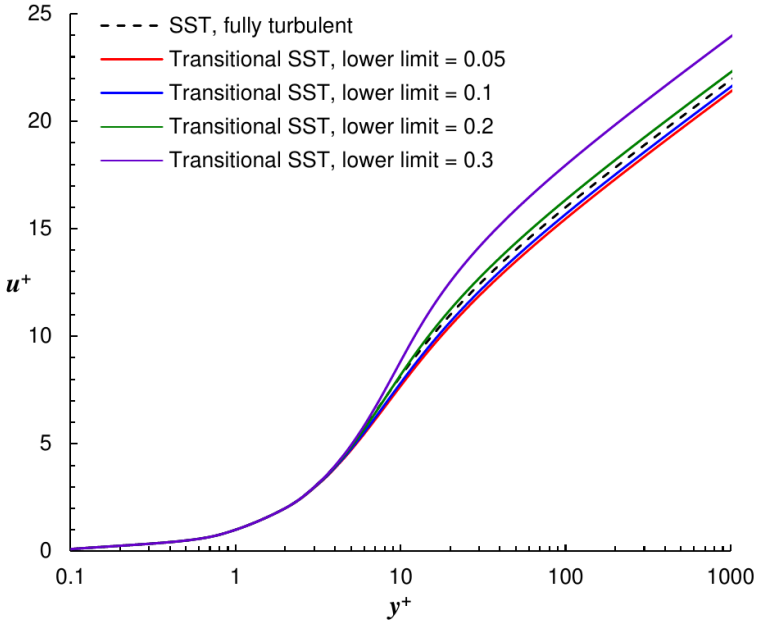

Figure 3.1: Turbulent boundary layer non-dimensional velocity distribution of $\gamma - Re_\theta$ model for varying destruction limiter constant. Reproduced from Coder and Maughmer [30].

3.2.2.2 Intermittency Limiter

Another limiter given in Eq. 3.41 is used to prevent the intermittency function ϕ from dropping below some critical level. This limiter implicitly exists in transport equation

models, too. For example, the intermittency equation in $\gamma - Re_\theta$ model of Langtry and Menter [8] and the γ model of Menter et al. [2] reads as Eq. 3.43

$$\frac{\partial(\rho\gamma)}{\partial t} + \frac{\partial(\rho U_j \gamma)}{\partial x_j} = P_\gamma - E_\gamma + \frac{\partial}{\partial x_j}\left[\left(\mu + \frac{\mu_t}{\sigma_\gamma}\right)\frac{\partial \gamma}{x_j}\right] \tag{3.43}$$

where the destruction term E_γ is defined as in Eq. 3.44

$$E_\gamma = c_{a2}\rho\Omega\gamma F_{turb}(c_{e2}\gamma - 1) \tag{3.44}$$

Here the constant c_{e2} determines the lower limit for the intermittency factor. γ model of Menter et al. [2] and $\gamma - Re_\theta$ model of Langtry and Menter [8] do not make the intermittency γ absolute zero in laminar regions but allow it to have a small value ($1/c_{e2}$ where $c_{e2} = 50$). Ströer et al. [72] investigated the stability behavior of $\gamma - Re_\theta$ model and pointed out that γ takes a small value but $\neq 0$ inside the laminar boundary layer to avoid an unstable solution.

If one sets a too high lower limit for the intermittency function ϕ, then the transition onset location moves upstream because of undamped excessive turbulence production. Similarly, if this limit is removed, then the stability of the model is affected, and even if one could get a converged result, the transition would be downstream. If one removes the destruction limiter, then the turbulence would not build up enough to recover fully turbulent behavior after the transition, and the stability issues would cause either oscillation in the solution or divergence. Even if a converged solution is obtained, forces in a fully turbulent region would not be correctly estimated.

3.3 Model Calibration

The present model includes only four constants needed to be calibrated, i.e., C_1, C_2, C_3,and C_{sep}. First of them, C_1, appears in $Term1$, Eq. 3.11, and is actually not significant as much as the others are. It is set to a high value to ensure $Term1$ is turned on once the onset of transition is detected. Since the current model is an abrupt model which neglects the transition length, the main consideration for $Term1$ is not how gradual transition is enabled but whether it is activated or not.

The main functionality of the model is controlled by C_2 and C_3 constants. In addition to them, C_{sep} has only a secondary purpose that sets a limit for the correction in

separated flows. C_2 appeared in $Term2$, Eq. 3.11, determines how strong $Term2$ is to be effective. C_3 in Eq. 3.41 is responsible for setting a lower limit for the intermittency function ϕ. C_2 and C_3 are calibrated against two zero pressure gradient flat plate cases, and then, C_{sep} is calibrated against an airfoil test case for only one angle of attack.

An important note here to be stated is that there are only a handful of detailed experimental data. Therefore, the fewer coefficients to be calibrated are favorable so that the calibration would be made using less experimental data, and the validation studies can be performed using the rest of the data. In the present model, the test cases are separated for their purpose of use. Each constant is calibrated against only one test case, and the model is validated against the other cases.

Initial numerical experiments showed the results for the Schubauer and Klebanoff (S&K) flat plate case [73] are independent of which C_2 value is chosen, so S&K case is used to determine a convenient interval for C_3. The denominator of C_3 is decreased gradually, and the transition onset location is monitored. In Fig. 3.2, different transition onset locations can be seen for varying C_3. The yellow shaded area represents the interval for gradual increments $C_3 = 1/100$ up to $C_3 = 1/20$. The figure also includes the results obtained using other models, the SA-BCM model of Cakmakcioglu et al. [22] and the γ model of Menter et al. [2], for comparison. As the lower limit of the intermittency function is raised, the transition onset location moves upstream. However, its behavior suddenly changes after $C_3 = 1/20$ by showing more sensitivity to the constant chosen, and that is even more obvious comparing to $C_3 = 1/10$, as the change of the former constant to the latter causes a significant shift in the transition onset location. Therefore, it seems $C_3 = 1/20$ is a proper limit for a stable transition onset to avoid unexpected behaviors.

After C_3 is fixed, C_2 is determined using T3B flat plate case. The same method is followed, and C_2 is gradually decreased as the transition onset location is monitored. As C_2 takes a lower value, the transition onset location moves downstream. $C_2 = 0.1$ is seen as suitable for optimum calibration.

Finally, C_{sep} is calibrated against the E387 low Reynolds number airfoil test case with laminar separation. We have used only zero angle of attack. The calibration param-

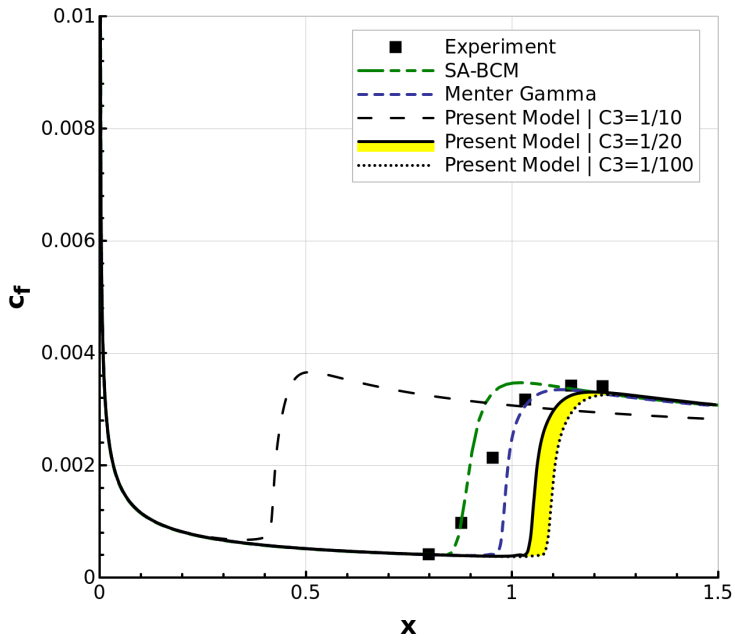

Figure 3.2: Skin friction coefficients of S&K flat plate case for varying C_3 constant

eters are the laminar separation bubble (LSB) size and, thus, drag coefficient c_d. In Fig. 3.3a, the pressure coefficient distribution for the E387 airfoil case is given with varying C_{sep} values. The major differences appear in the separation bubble region, and it is hard to notice them in full view, so a close-up detail of the separation bubble region is presented in Fig. 3.3b. As C_{sep} value is the upper limit of exaggerated intermittency at the end, it determines how strongly the separation correction is to be effective. The higher the separation correction constant C_{sep}, the smaller the separation bubble size. Value of C_{sep} is gradually increased from 2 to 3 in order to find the optimum point. Fig. 3.3b shows the behavior of the model. Because the effect of increments between 2 to 2.5 and between 2.6 to 3 is hard to notice for each step, those regions are presented as shaded areas, gray for the former and yellow for the latter. In those two regions, a reasonable gradual trend is seen while an interesting jump is came across during the increment from 2.5 to 2.6. The model is seen to be highly sensitive the values between 2.5 and 2.6; therefore, it is suggested to avoid C_{sep} to take a value in this interval.

In Table 3.1, aerodynamic coefficients, i.e., lift coefficient c_l and drag coefficient c_d, computed using the current transition model are listed for each C_{sep} value. Percent error compared to experimental data is also given. As mentioned before, the interval

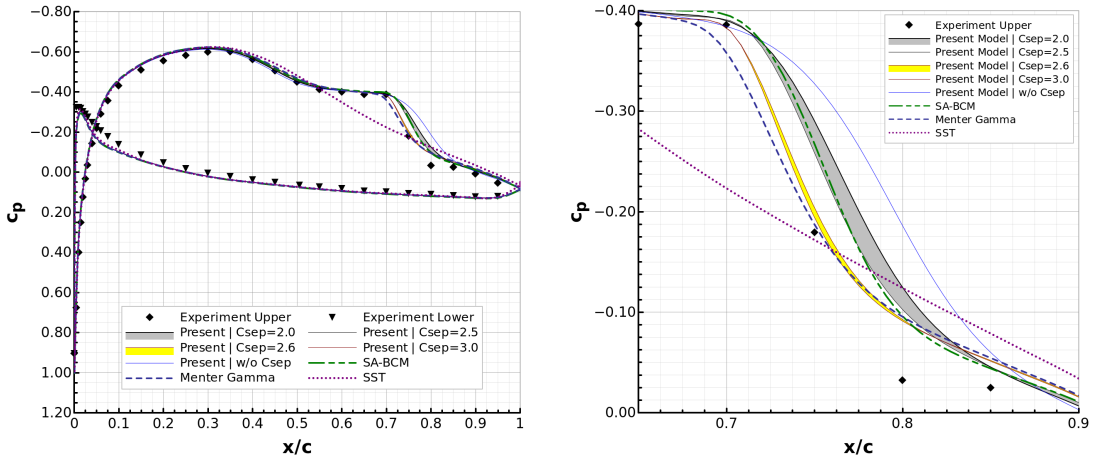

(a) Full view

(b) Close-up view

Figure 3.3: Pressure coefficient distribution for E387 airfoil case at $0°$AoA with varying C_{sep}

between 2.5 and 2.6 is avoided, and $C_{sep} = 2.7$ is considered safer to prefer, given the equity of results for $C_{sep} = 2.6$ and $C_{sep} = 2.7$. Thus, $C_{sep} = 2.7$ is chosen to be the optimum point providing reasonable accuracy.

The pressure coefficient distribution for the E387 airfoil case with and without separation correction is given in Fig. 3.4. Again, the results for the other transition models, the SA-BCM model of Cakmakcioglu et al. [22] and the γ model of Menter et al. [2], and also results for fully turbulent SST model are included in the figure for comparison. In Table 3.2, the aerodynamic coefficients are also given for all mentioned models. Current calibration makes the behavior of the transition model closer to the γ model and provides a better prediction of the bubble size than the SA-BCM model does.

Table 3.1: Aerodynamic coefficients of E387 airfoil computed using current transition model for different C_{sep} values

	c_l	Error (%)	c_d	Error (%)
Experiment	0.352	-	0.0105	-
without C_{sep}	0.394	11.93	0.0115	9.52
$C_{sep} = 2.0$	0.391	11.08	0.0109	3.81
$C_{sep} = 2.1$	0.390	10.80	0.0109	3.81
$C_{sep} = 2.2$	0.390	10.80	0.0108	2.86
$C_{sep} = 2.3$	0.390	10.80	0.0108	2.86
$C_{sep} = 2.4$	0.390	10.80	0.0108	2.86
$C_{sep} = 2.5$	0.390	10.80	0.0107	1.90
$C_{sep} = 2.6$	0.388	10.23	0.0104	0.95
$\boldsymbol{C_{sep} = 2.7}$	**0.388**	**10.23**	**0.0104**	**0.95**
$C_{sep} = 2.8$	0.387	9.94	0.0103	1.90
$C_{sep} = 2.9$	0.387	9.94	0.0103	1.90
$C_{sep} = 3.0$	0.387	9.94	0.0103	1.90

Table 3.2: Aerodynamic coefficients of E387 airfoil computed with different models

	c_l	Error (%)	c_d	Error (%)
Experiment	0.352	-	0.0105	-
Fully Turbulent SST Model	0.375	6.53	0.0138	31.43
SA-BCM Model [22]	0.396	12.50	0.0103	1.90
γ Model of Menter et al. [2]	0.388	10.23	0.0104	0.95
Transition Model with $\boldsymbol{C_{sep} = 2.7}$	**0.388**	**10.23**	**0.0104**	**0.95**
Transition Model without C_{sep}	0.394	11.93	0.0115	9.52

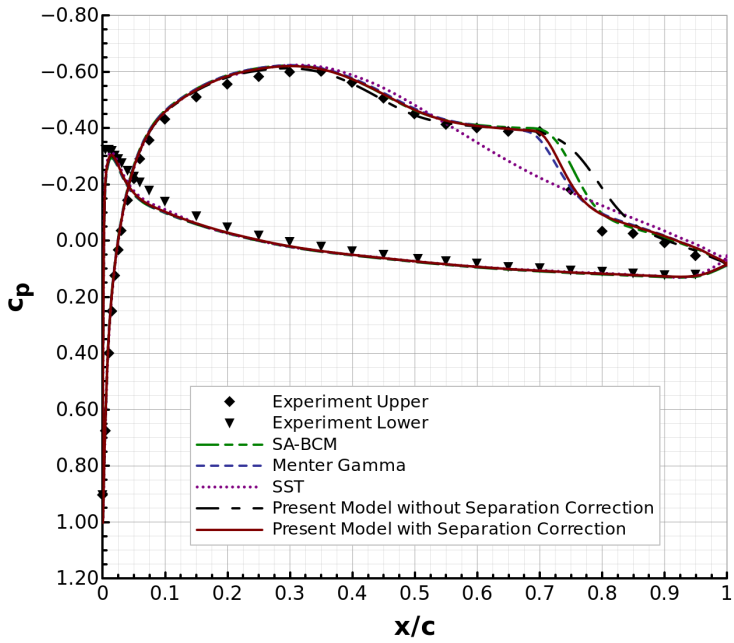

Figure 3.4: Pressure coefficient distribution for E387 airfoil case at 0°AoA

CHAPTER 4

VALIDATION

In this chapter, validation studies are given. First of all, the flow solver is introduced, and the numerical settings are summarized. Then, the results obtained for ERCOFTAC T3 series experimental flat plate cases [31] are given. Both zero and non-zero pressure gradient cases are solved using the proposed model. In addition, results for the Eppler E387 and the NLF(1)-0416 airfoil cases are also presented.

4.1 Flow Solver

All developments presented in this thesis are performed using an open-source density-based solver $FlowPsi$, developed by Luke et al. [74]. $FlowPsi$ is capable of dealing with general unstructured grids and uses a cell-centered finite-volume formulation. It offers various flux schemes and allows both explicit and implicit temporal discretizations. Several Gauss-Seidel-based linear system solvers come with the $FlowPsi$ package, and techniques such as local-time-stepping, relaxation, and preconditioner are used to improve the solver's performance.

All results presented in the thesis are obtained using the following settings. Inviscid fluxes are discretized using the HLLC scheme of Toro et al. [75], and the MUSCL reconstruction [76] is used for face-state extrapolations. The line-symmetric Gauss-Seidel (LSGS) method is used as a linear system solver, and a preconditioning technique is applied to improve the solver performance at low Mach numbers.

$FlowPsi$ offers several RANS turbulence models, including Spalart-Allmaras (SA) [21], Realizable k-ϵ [77], k-ω [55], k-ω SST [28]. However, it provides only three

equation k_T-k_L-ω model of Walters and Cokljat [52] among the transition sensitive models. Therefore, the author implemented the SA-BCM model of Cakmakcioglu et al. [22] and the γ model of Menter et al. [2] into the solver for comparison purposes. The current transition model is also implemented into the solver in the scope of thesis work.

4.2 Flat Plate Test Cases

The present model is validated against the ERCOFTAC (European Research Community on Flow, Turbulence, and Combustion) T3 series of experimental flat plate test cases,[31] which are widely used for validation of any transition model in the literature due to their well-documented data and their relevance to practical engineering applications. The experiments conducted on a 1.5-meter-long flat plate provide data for flows with various free-stream velocities and turbulence intensities. The cases have a free-stream turbulence intensity varying from 0.9% to 6.0%, mostly around 3%, which makes them host bypass transition. The tunnel's adjustable top wall is used to generate a pressure gradient, such that some cases are considered representative of turbine blade loading with streamwise pressure gradient and high turbulence intensity. For natural transition mode, the Schubauer and Klebanoff (S&K) experimental flat plate case [73] is an example with a free-stream turbulence intensity of 0.03%, so it is also used to validate the present model. The test cases and inlet conditions at the leading edge of the plate are listed in Table 4.1. Note that these are conditions at the leading edge of the plate, and the domain inlet boundary condition is a bit higher than these values. It can be calculated by solving the standard k-ω SST model turbulence intensity decay formulation given in Eq. 4.1.

$$Tu_{LE} = \sqrt{Tu_{inlet}^2 \cdot \left(1 + \frac{3 \cdot \rho \cdot V \cdot x \cdot \beta \cdot Tu_{inlet}^2}{2 \cdot \mu \left(\mu_t / \mu\right)}\right)^{-\frac{\beta^*}{\beta}}} \tag{4.1}$$

where $\beta^* = -0.0828$ and $\beta = 0.09$ which are constants of SST model in the free-stream, ρ is fluid density, μ_t is eddy viscosity which equals to $\rho k/\omega$, x is the streamwise distance to the leading edge, V is the mean convective velocity, and LE subscript is an acronym for leading edge.

The inlet conditions are defined to match free-stream turbulence intensity decay over the plate with the experiments. For all flat plate cases, constant air properties are assumed with a density of $\rho = 1.2\ \mathrm{kg/m^3}$ and a dynamic viscosity of $\mu = 1.8 \times 10^{-5}$ $\mathrm{Pa.s}$.

Table 4.1: Test cases and inlet conditions at the leading edge of the plate

Case	$u\ [m/s]$	$Tu\ [\%]$	μ_t/μ
S&K	50.1	0.03	1
T3A-	19.8	0.93	8
T3A	5.4	3.3	12
T3B	9.4	6	100
T3C2	5.05	3	8
T3C3	3.85	3	5
T3C4	1.348	3	2
T3C5	8.54	3	15

4.2.1 Grid Independence Study

For zero pressure gradient flat plate cases, two rectangle domains are formed. The no-slip wall is 1.5-meter-long for S&K, T3A, and T3B cases, while a 1.7-meter-long wall is generated for T3A- case. For both domains, the top boundary is placed 0.5 m above the flat plate, and the vertical inlet plane is 0.04 m ahead of the leading edge of the no-slip wall. Slip wall boundary condition is used for the top boundary and the distance between the inlet plane and the flat plate. For the inlet plane, uniform velocity inflow condition is defined, and for the outlet plane, 1 atm pressure outlet boundary condition is imposed. The boundary conditions and domain dimensions are represented in Fig. 4.1. For T3A- case, the no-slip wall is 1.7-meter-long, which is the only difference from Fig. 4.1.

The generated grids are sufficiently refined using five levels of grids. Refinement for the grid with 1.5-meter-long wall is made using the S&K case, as it has the highest Reynolds number flow among zero pressure gradient flat plate cases. The details for grids with 1.5-meter-long wall are listed in Table 4.2. Drag coefficient convergence

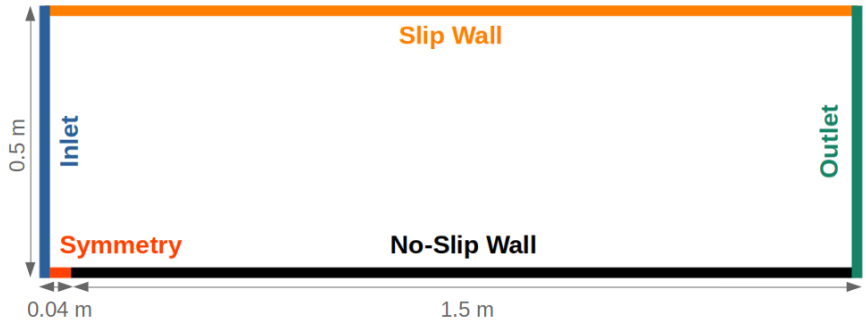

Figure 4.1: Boundary conditions for zero pressure gradient flat plate cases

with respect to grid spacing h is shown in Fig. 4.2, and skin friction coefficient distributions for different level grids are also given in Fig. 4.3.

Table 4.2: 1.5-meter-long zero pressure gradient flat plate grid details

	Number of nodes (X × Y)	Grid spacing h
Level 1	479×240	2.95×10^{-3}
Level 2	359×160	4.17×10^{-3}
Level 3	239×120	5.90×10^{-3}
Level 4	179×80	8.36×10^{-3}
Level 5	119×60	11.83×10^{-3}

The details of grids generated with 1.7-meter-long wall are listed in Table 4.3. Drag coefficient convergence with respect to grid spacing h is shown in Fig. 4.4, and skin friction coefficient distributions for different level grids are also given in Fig. 4.5.

Table 4.3: 1.7-meter-long zero pressure gradient flat plate grid details

	Number of nodes (X × Y)	Grid spacing h
Level 1	679×270	2.34×10^{-3}
Level 2	509×180	3.30×10^{-3}
Level 3	339×120	4.96×10^{-3}
Level 4	224×80	7.47×10^{-3}
Level 5	119×60	11.83×10^{-3}

From Fig. 4.3 and 4.5, it can be noticed that Level 3 grids approximately find the transition location, and the correct location is estimated after Level 2 grids. The dif-

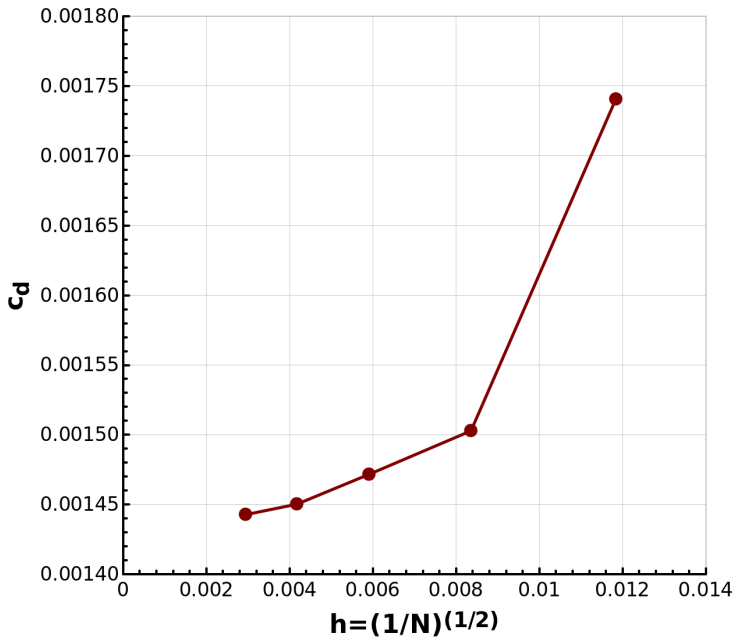

Figure 4.2: Drag coefficient convergence for S&K flat plate case

ference between Level 2 and Level 1 grids is the steepness of the transition, which is the main effect that causes drag coefficients to vary. Therefore, oscillatory convergence in T3A- case, seen in Fig. 4.4, should not pose a serious problem. Recall that the main concern is to estimate the transition location, and the current model has no means to estimate transition length that is not aimed to be found out.

The chosen grid for T3A- case has 509×180 nodes in x and y directions, respectively, and the grid for other zero-pressure flat plate cases has 359×160 nodes. As $FlowPsi$ is a 3-dimensional solver, one cell depth in z-direction is used. For both grids, other grid parameters are the same: the first wall-normal node height of 1×10^{-5} m, the first streamwise grid step of 10^{-3} m from the leading edge of the plate and the expansion ratio of 1.05 in both wall-normal and streamwise directions. These parameters guarantee $y^+ < 1$ for all cases.

As for flat plate cases with pressure gradient (T3C series), a domain with 2-meter-long flat plate is generated. The vertical inlet plane is again at 0.04 m ahead of the leading edge of the plate. However, the top boundary is not a horizontal line anymore but a curve to impose the streamwise pressure gradient as in the experiment. For each T3C case, the coordinates of the upper boundary are defined to match experimental free-

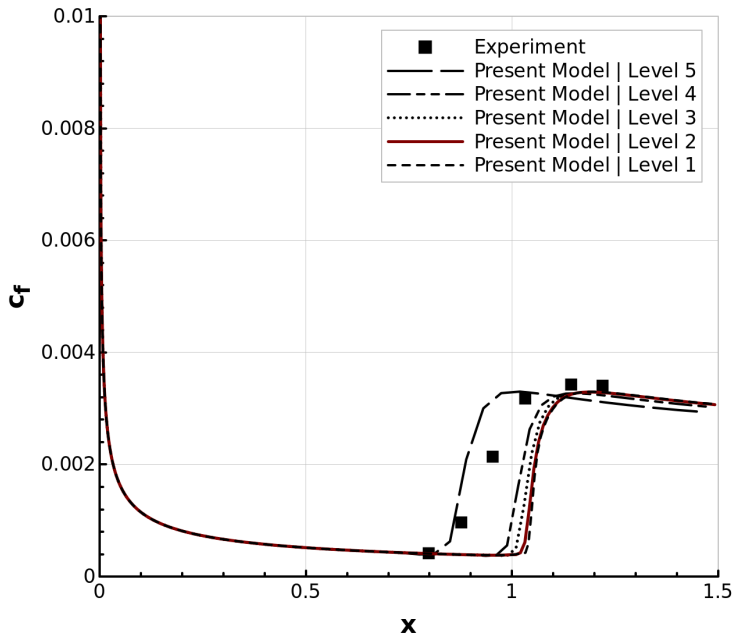

Figure 4.3: Skin friction coefficient distributions of different level grids for S&K flat plate case

stream velocity distribution over the plate. The generated upper boundary profiles are pretty much the same of that Menter et al. [2] used. For all T3C cases, the grid has $568 \times 140 \times 2$ nodes in x, y, and z directions, respectively, and the first wall-normal node is placed at 2×10^{-5} m, ensuring y^+ values lower than unity. Other parameters are the same with grids used for zero pressure gradient flat plates.

4.2.2 Results for Zero Pressure Gradient Test Cases

The skin friction coefficients of zero pressure gradient flat plate cases (S&K, T3A-, T3A, T3B) are shown in Fig. 4.6. Results for the SA-BCM model of Cakmakcioglu et al. [22] and γ model of Menter et al. [2] are also included. The present model represents the proposed model of this thesis. The results show a good agreement with the experimental data, though an exception for T3A- may be noted. For all cases, the transition behavior of the current algebraic model is very close to the γ model of Menter et al. [2]. It may be desirable as the correlations and base turbulence model used are eventually the same, even though the transition modeling approaches differ.

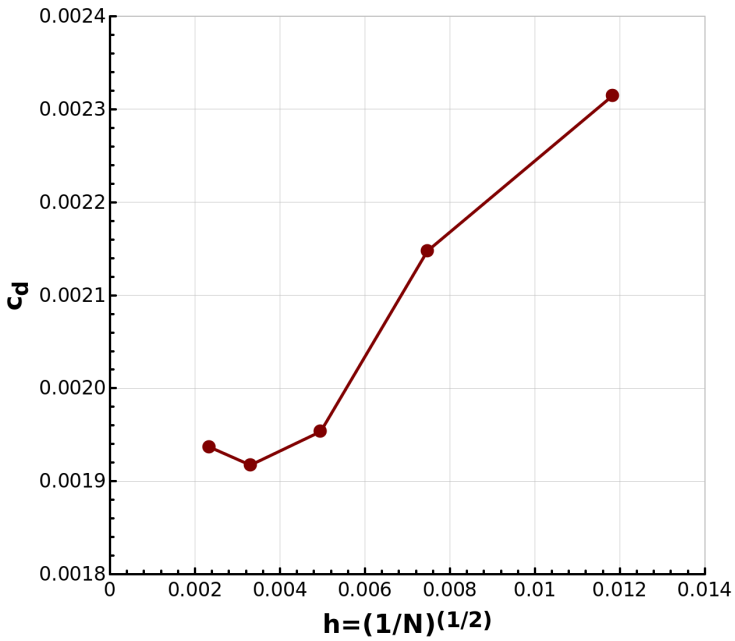

Figure 4.4: Drag coefficient convergence for T3A- flat plate case

4.2.3 Results for Pressure Gradient Test Cases

Fig. 4.7 shows the skin friction coefficients of flat plate cases with pressure gradient (T3C2, T3C3, T3C4, T3C5). For all cases, the results of the current algebraic model are competitive with the γ model of Menter et al. [2] despite its reduced order nature. The results demonstrate the present approach is a good alternative to transport equation models.

An interesting point that may be noticed is the transition length performance of the current model compared to other algebraic models. Although the current approach does not aim for any estimation of the transition length at all, it seems the current model estimates the transition length better than the k_γ model of Sandhu and Ghosh [26] and the algebraic γ model of Menter et al. [27], given the results they presented. It is known that algebraic models tend to make steeper transitions compared to transport equation models [26]. This phenomenon can be seen in both aforementioned algebraic models, especially in T3A and T3C5 test cases. The present model makes a smoother transition in those test cases, as seen in Fig. 4.6 and 4.7, so it may be favorable in that aspect.

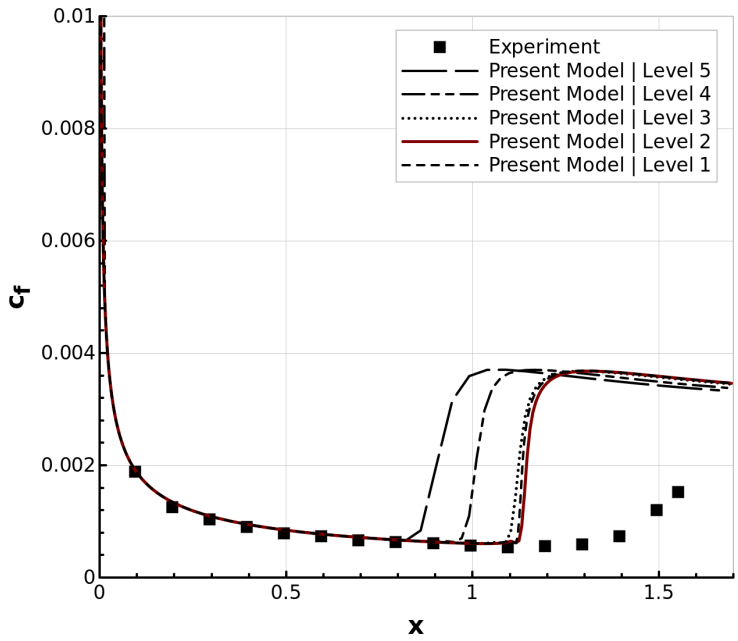

Figure 4.5: Skin friction coefficient distributions of different level grids for T3A- flat plate case

4.3 Eppler E387 Airfoil Case

Eppler E387 airfoil is one of the well-known benchmark cases in transition modeling. McGhee et al. [78] tested the Eppler 387 airfoil in the Langley Low-Turbulence Pressure Tunnel (LTPT) and provided detailed experimental data over Mach number range from 0.03 to 0.13 and a chord Reynolds number range from 60,000 to 460,000. For validation, the flow at $M = 0.06$ and $Re = 200,000$ is solved for different angles of attacks, and compared with the experimental results.

The computational domain shown in Fig. 4.8 is generated as an O-type grid with dimensions of 708x181. First cell thickness is set to be 10^{-5} units to ensure $y+ < 1$ over the surface, and the cell sizes are expanded with a ratio of 1.075 through the far field. The boundary conditions are set to match experimental conditions at $M = 0.06$, $Re = 200,000$, and $P_t = 15$ psi. Inlet conditions for turbulence variables are determined using $Tu = 0.09\%$ and $\mu_t/\mu = 12$.

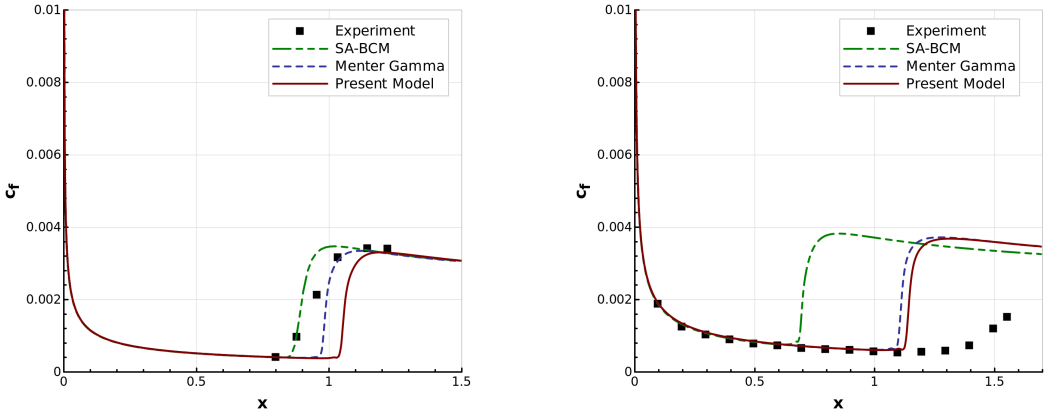

(a) S&K (b) T3A-

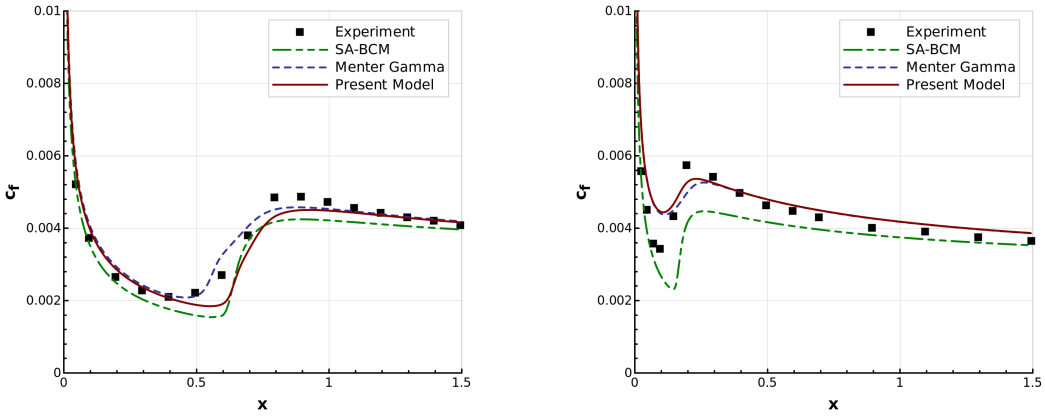

(c) T3A (d) T3B

Figure 4.6: Skin friction coefficients for zero pressure gradient flat plate cases

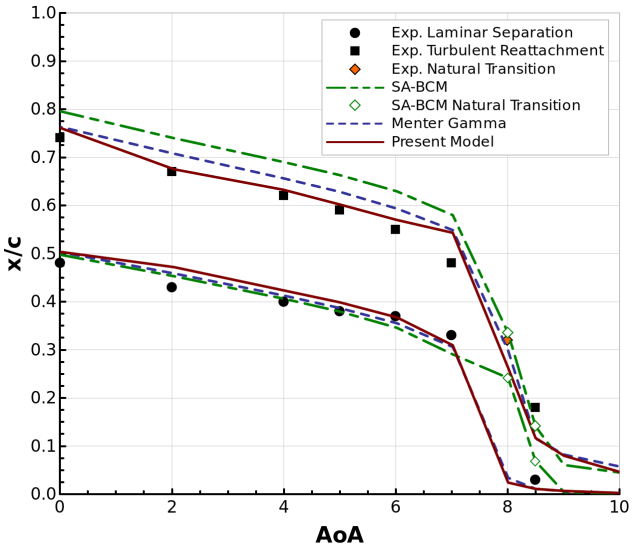

Figure 4.9: Flow map on the suction side for Eppler E387 airfoil

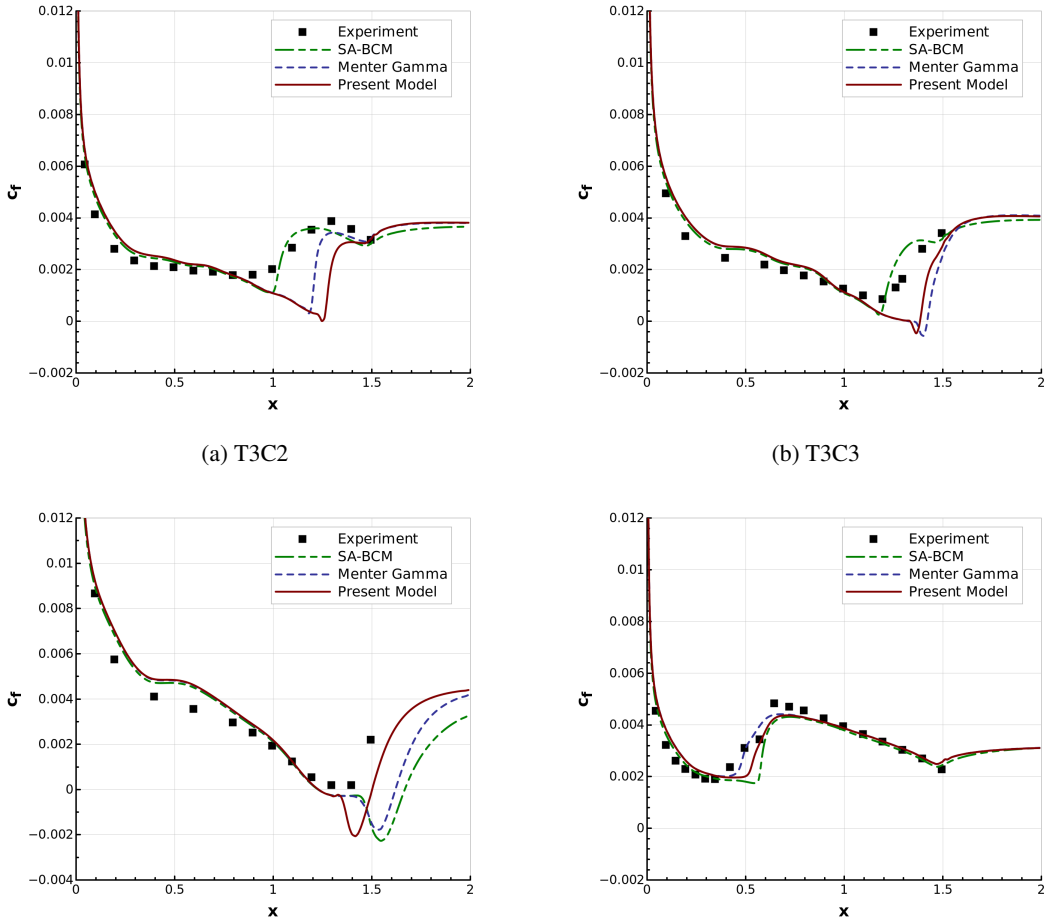

(a) T3C2

(b) T3C3

(c) T3C4

(d) T3C5

Figure 4.7: Skin friction coefficients for variable pressure gradient flat plate cases

The flow map on the suction surface is presented in Fig. 4.9. The current transition model finds laminar separation bubble sizes consistent with the experimental data. Although the results obtained using the γ model and SA-BCM are similar, the present model provides a better estimation of turbulent reattachment. An exception at the 8-degree angle of attack may be noticed as the experiments show the flow is attached and the transition mode is through the natural transition. However, the present model still predicts a separation bubble. A similar problem is observed in the γ model and other transition models by Menter et al. [27], too. Interestingly, SA-BCM finds the correct transition mode at 8-degree angle of attack and shows that the flow does not separate. However, SA-BCM again estimates a natural transition at 8.5-degree angle of attack in contrast to the experimental results.

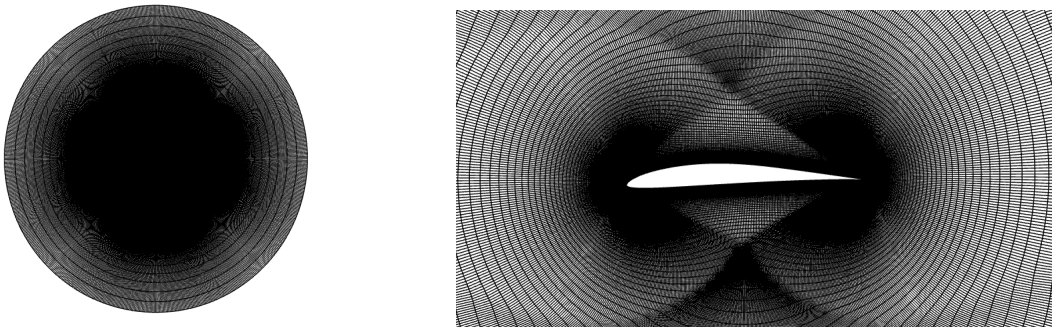

(a) O-grid

(b) Grid zoomed in

Figure 4.8: Computational domain for Eppler E387

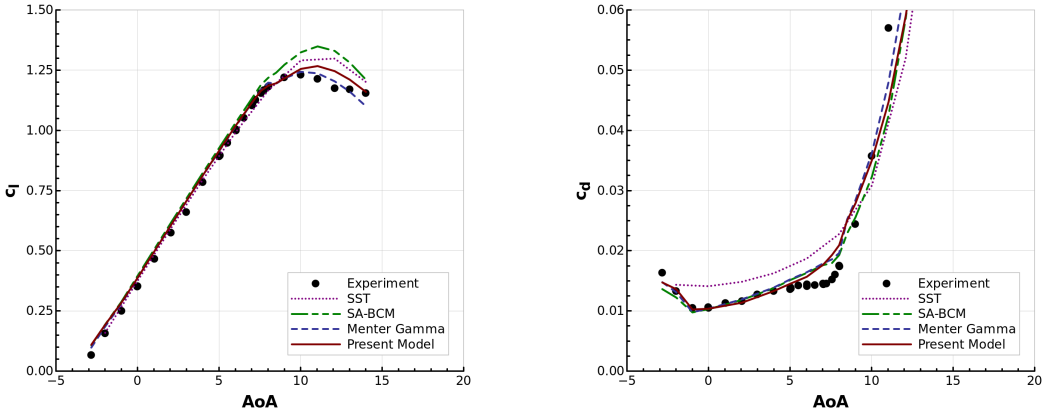

(a) Lift coefficient

(b) Drag coefficient

Figure 4.10: Aerodynamic coefficients versus angle of attack graphs for Eppler E387 airfoil

In Fig. 4.10, lift and drag coefficients versus angle of attack are given. The present model predicts the maximum lift coefficient better than the fully turbulent SST model and the SA-BCM model. Results are almost identical to the γ model except at the region between 10 and 15 angles of attack, where the γ model estimates the lift coffi-cient more accurate. The main advantage of the present model compared to the fully turbulent SST model appears in the prediction of the drag coefficient, as it takes into account laminar portions of flow and the presence of the separation bubbles. While the other transition models give similar results, the current model shows slightly bet-ter behavior than theirs. Fig. 4.11 shows the lift-drag polar. The present model accurately predicts the drag bucket and clearly outperforms the fully turbulent SST model. The behaviors of the current model and the γ model are very close, while the

SA-BCM model significantly deviates after the maximum lift point.

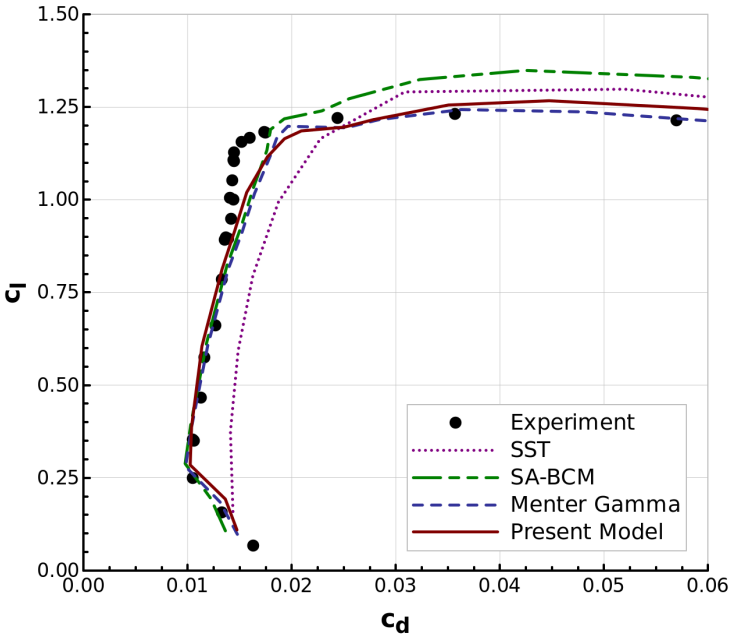

Figure 4.11: Lift-drag polar curves for Eppler E387 airfoil

4.4 NLF(1)-0416 Airfoil Case

The Natural Laminar Flow NLF(1)-0416 airfoil is an airfoil designed for general aviation applications. This airfoil was tested at NASA Langley Research Center, and the experimental results were reported by Somers [79]. The experimental flow conditions for the validation are $M = 0.1$ and $Re = 4,000,000$.

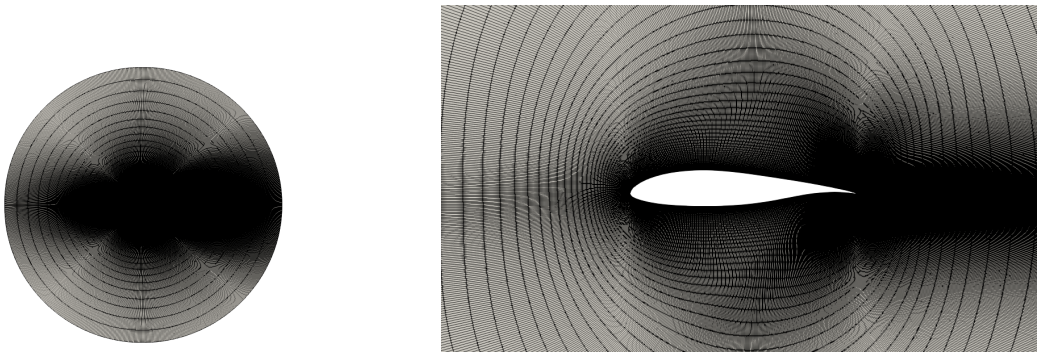

(a) O-grid

(b) Grid zoomed in

Figure 4.12: Computational domain for NLF(1)-0416

An O-type grid is generated for the computational domain shown in Fig. 4.12. Each surface of the airfoil have 500 points and the grid is expanded 164 points with an expansion ration of 1.1 through the far field. The first cell thickness is set to be 3.5×10^{-6} units considering a $y+ < 1$ criterion over the surface. The boundary conditions are set to match experimental conditions. Inlet conditions for turbulence variables are determined using $Tu = 1\%$ and $\mu_t/\mu = 90$, the values which resulted in approximately 0.1% turbulence intensity near the leading edge of the airfoil.

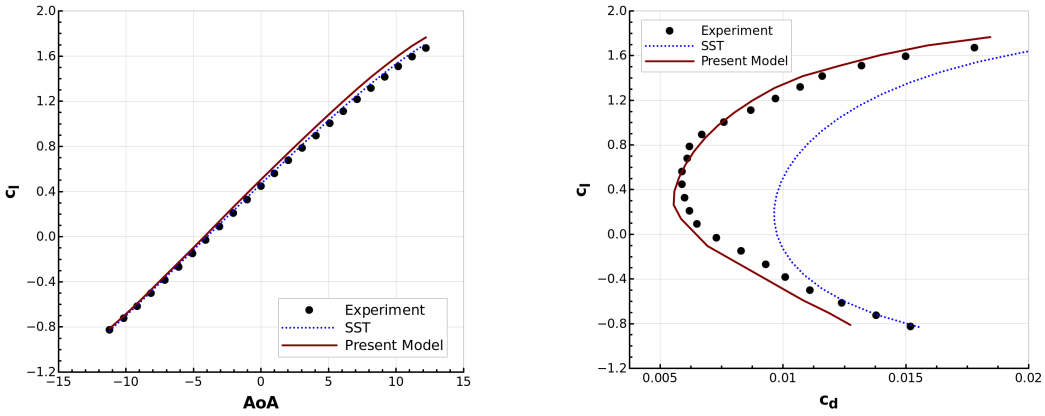

(a) Lift coefficient versus angle of attack

(b) Lift-drag polar curve

Figure 4.13: Aerodynamic coefficients for NLF(1)-0416 airfoil

Fig. 4.13 gives the lift coefficient versus the angle of attack graph and lift-drag polar. The present model estimates the drag bucket quite well and better than fully turbulent SST model. Similar to Eppler E387 case, the lift coefficient is overpredicted as the angle of attack is increased. However, the improvement in drag coefficient predictions balances this behavior. An interesting point can be noticed and noted here that the behavior in negative angles of attack is simply the opposite of the case seen in positive angles. As far as the negative angles of attack are concerned, the drag coefficient is underpredicted, while the lift coefficient estimations very closely fit the experimental data. After all, although some overpredictions and underpredictions are seen, the error band is narrow.

CHAPTER 5

CONCLUSION

In this thesis, a new correlation-based transition model is proposed. The model employs an algebraic intermittency function that controls the source terms of the underlying turbulence model and entirely relies on local variables. The proposed model is developed based on the ideas of Baş et al. [20] that the transition can be modeled using a proper algebraic intermittency function without any need for solving additional transport equation or equations.

The intermittency function used in the present model is a heavily modified version of that in the SA-BCM model [20, 22], and it is coupled with the $k-\omega$ SST turbulence model [28, 29] to remedy the shortcomings of the SA-BCM model, particularly the lack of the calculation of the turbulence intensity decay along the domain. The present model preserves the main form of the SA-BCM intermittency function, i.e., the dependency on only two terms, $Term1$ and $Term2$. The former term, $Term1$, depends on the correlation and starts the transition onset. The latter term, $Term2$, is responsible for diffusing the turbulent flow into the depth of the boundary layer. However, the formulations are not the same of the SA-BCM model. $Re_{\theta c}$ correlation in $Term1$ is replaced with the one suggested by Menter et al. [2] to use local turbulence intensity definition. $Term2$ is similar to that in the SA-BCM model, but its form is changed in the present model to avoid a fully turbulent solution.

Some modifications are made to enable a robust coupling with k-ω SST model. The destruction term of the turbulent kinetic energy equation is limited depending on the value that the intermittency function takes. In addition, the intermittency function is forced not to drop below a small minimum value to guarantee the stability and reliability of the model. Assessment of these limiters is also given in the thesis.

A new separation correction term is proposed to improve separation-induced transition predictions. This correction compensates the insufficient turbulence production of k-ω SST model to reattach the flow in case of separation. The prominent feature of the proposed correction is that it does not introduce any new functions but relies on the already calculated terms. Therefore, it does not impose a substantial burden on the model.

One of the objectives of the present model is to keep it as simple as possible. This concern is mainly because of avoiding the use of too many cases to make a proper calibration. As the detailed experimental data is scarce, having fewer coefficients would be better. In the development of the model, it is strictly avoided to calibrate a parameter by using more than one case. In other words, each parameter is calibrated against one case, and the model is validated against the other test cases. The model has only four parameters that need to be calibrated, and the calibration procedure is explained in the related section.

The present model is implemented in an open-source flow solver and validated using well-known ERCOFTAC flat plate cases. The results show a good agreement with the experimental data in both cases with zero pressure gradient and with non-zero pressure gradient. In addition, an low Reynolds number airfoil case, Eppler E387, and a natural laminar flow airfoil, NLF(1)-0416, are used for the validation, and the model gives very promising results by accurately predicting the drag bucket and the separation bubble length.

1-equation γ model [2] and algebraic SA-BCM model are also implemented for comparison reasons. The results obtained from these models are given in the corresponding figures. Overall, the present model gives results close to the γ model and competitive compared to the SA-BCM model.

The findings of this thesis demonstrate that the present model is a promising alternative for capturing boundary layer transition effects in daily industrial CFD problems. The model significantly reduces the number of constants and functions required compared to existing one- or two-equation transition models. The model's ability to provide reasonably accurate results with reduced computational cost makes it a valuable means for engineers and researchers seeking to capture complex flow phenomena

without compromising accuracy or computational efficiency.

The model proposed in the thesis can capture different transition modes, i.e., natural, bypass, and separation-induced. For future work, its capabilities can be extended to handle diverse transitional flows by involving the effects of cross-flow instabilities and compressibility. In addition, current correlations only provide the effects of turbulence intensity and pressure gradient to the model. Although these are the main parameters affecting the transition and sufficient in most cases, it would be appealing to include the surface roughness effects. This thesis does not present any three-dimensional application, which may be seen as a deficiency. Future work involves exploring the applications of a wide range of challenging three-dimensional cases.

It should be remembered that the current approach relies on correlations to predict the transition, and the limits of its ability will always be drawn by the correctness of the correlations. As the parameters affecting the transition are more precisely taken into account by the correlations, the error sources will be reduced. Therefore, one side of the modeling will always depend on the realization of more accurate experiments in the future.

REFERENCES

[1] M. S. Genc, I. Karasu, H. H. Acikel, and M. T. Akpolat, "Low reynolds number flows and transition," in *Low Reynolds Number* (M. S. Genc, ed.), ch. 1, Rijeka: IntechOpen, 2012.

[2] F. R. Menter, P. E. Smirnov, T. Liu, and R. Avancha, "A one-equation local correlation-based transition model," *Flow, Turbulence and Combustion*, vol. 95, no. 4, pp. 583–619, 2015.

[3] J. Van Ingen, "A suggested semi-empirical method for the calculation of the boundary layer transition region," Rep. VTH-74, University of Delft, Dept. of Aerospace Engineering, Delft, The Netherlands, 1956.

[4] A. Smith and N. Gamberoni, "Transition, pressure gradient and stability theory," Rep. ES 26388, Douglas Aircraft Company, Long Beach, California, USA, 1956.

[5] F. R. Menter, R. B. Langtry, S. R. Likki, Y. B. Suzen, P. G. Huang, and S. Völker, "A Correlation-Based Transition Model Using Local Variables—Part I: Model Formulation," *Journal of Turbomachinery*, vol. 128, pp. 413–422, 3 2006.

[6] F. Menter, T. Esch, and S. Kubacki, "Transition modelling based on local variables," in *Engineering Turbulence Modelling and Experiments 5* (W. Rodi and N. Fueyo, eds.), pp. 555–564, Oxford: Elsevier Science Ltd, 2002.

[7] F. Menter, R. Langtry, S. Völker, and P. Huang, "Transition modelling for general purpose CFD codes," in *Engineering Turbulence Modelling and Experiments 6* (W. Rodi and M. Mulas, eds.), pp. 31–48, Amsterdam: Elsevier Science B.V., 2005.

[8] R. B. Langtry and F. R. Menter, "Correlation-based transition modeling for unstructured parallelized computational fluid dynamics codes," *AIAA Journal*, vol. 47, no. 12, pp. 2894–2906, 2009.

[9] W. Jones and B. Launder, "The calculation of low-reynolds-number phenomena with a two-equation model of turbulence," *International Journal of Heat and Mass Transfer*, vol. 16, no. 6, pp. 1119–1130, 1973.

[10] H. W. Emmons, "The laminar-turbulent transition in a boundary layer-part i," *Journal of the Aeronautical Sciences*, vol. 18, no. 7, pp. 490–498, 1951.

[11] S. Dhawan and R. Narasimha, "Some properties of boundary layer flow during the transition from laminar to turbulent motion," *Journal of Fluid Mechanics*, vol. 3, no. 4, p. 418–436, 1958.

[12] J. Steelant and E. Dick, "Modelling of bypass transition with conditioned navier–stokes equations coupled to an intermittency transport equation," *International Journal for Numerical Methods in Fluids*, vol. 23, no. 3, pp. 193–220, 1996.

[13] Y. Suzen and P. Huang, "Modeling of flow transition using an intermittency transport equation," *Journal of Fluids Engineering, Transactions of the ASME*, vol. 122, no. 2, pp. 273–284, 2000.

[14] B. Abu-Ghannam and R. Shaw, "Natural transition of boundary layers - the effects of turbulence, pressure gradient, and flow history.," *Journal of Mechanical Engineering Science*, vol. 22, no. 5, pp. 213–228, 1980.

[15] R. Mayle, "The role of laminar-turbulent transition in gas turbine engines," *Journal of Turbomachinery*, vol. 113, no. 4, pp. 509–536, 1991.

[16] S. Cakmakcioglu, O. Bas, and U. Kaynak, "A correlation-based algebraic transition model," *Proceedings of the Institution of Mechanical Engineers, Part C: Journal of Mechanical Engineering Science*, vol. 232, no. 21, pp. 3915–3929, 2018.

[17] E. Van Driest and C. Blumer, "Boundary layer transition- freestream turbulence and pressure gradient effects," *AIAA Journal*, vol. 1, no. 6, pp. 1303–1306, 1963.

[18] E. Dick and S. Kubacki, "Transition models for turbomachinery boundary layer flows: A review," *International Journal of Turbomachinery, Propulsion and Power*, vol. 2, no. 2, 2017.

[19] R. B. Langtry, F. R. Menter, S. R. Likki, Y. B. Suzen, P. G. Huang, and S. Völker, "A Correlation-Based Transition Model Using Local Variables—Part II: Test Cases and Industrial Applications," *Journal of Turbomachinery*, pp. 423–434, 03 2004.

[20] O. Bas, S. Cakmakcioglu, and U. Kaynak, "A novel intermittency distribution based transition model for low-re number airfoils," in *31st AIAA Applied Aerodynamics Conference*, 2013.

[21] P. Spalart and S. Allmaras, "A one-equation turbulence model for aerodynamic flows," *AIAA Journal*, vol. 439, 01 1992.

[22] S. Cakmakcioglu, O. Bas, R. Mura, and U. Kaynak, "A revised one-equation transitional model for external aerodynamics," in *AIAA AVIATION 2020 FORUM*, vol. 1 PartF, 2020.

[23] R. Mura and S. Cakmakcioglu, "A revised one-equation transitional model for external aerodynamics-part i: Theory, validation and base cases," in *AIAA AVIATION 2020 FORUM*, vol. 1 PartF, 2020.

[24] U. Kaynak, O. Bas, S. C. Cakmakcioglu, and I. H. Tuncer, "Transition modeling for low to high speed boundary layer flows with CFD applications," in *Boundary Layer Flows* (V. R. Prasad, ed.), ch. 5, Rijeka: IntechOpen, 2020.

[25] J. Coder and M. Maughmer, "One-equation transition closure for eddy-viscosity turbulence models in CFD," in *50th AIAA Aerospace Sciences Meeting including the New Horizons Forum and Aerospace Exposition*, 2012.

[26] J. Sandhu and S. Ghosh, "A local correlation-based zero-equation transition model," *Computers & Fluids*, vol. 214, p. 104758, 2021.

[27] F. R. Menter, A. Matyushenko, R. Lechner, A. Stabnikov, and A. Garbaruk, "An algebraic LCTM model for laminar–turbulent transition prediction," *Flow, Turbulence and Combustion*, vol. 109, pp. 841–869, Nov. 2022.

[28] F. Menter, "Two-equation eddy-viscosity turbulence models for engineering applications," *AIAA Journal*, vol. 32, no. 8, pp. 1598–1605, 1994.

[29] F. Menter, M. Kuntz, and R. Langtry, "Ten years of industrial experience with the sst turbulence model," *Turbulence, Heat and Mass Transfer*, vol. 4, pp. 625–632, 2003.

[30] J. G. Coder and M. D. Maughmer, "Application of the amplification factor transport transition model to the shear stress transport model," in *53rd AIAA Aerospace Sciences Meeting*, 2015.

[31] A. Savill, "Some recent progress in the turbulence modeling of by-pass transition," *Near-Wall Turbulent Flows*, pp. 829–848, 1993.

[32] P. S. Klebanoff, K. D. Tidstrom, and L. M. Sargent, "The three-dimensional nature of boundary-layer instability," *Journal of Fluid Mechanics*, vol. 12, no. 1, p. 1–34, 1962.

[33] H. Schlichting, *Boundary Layer Theory*. McGraw-Hill, Inc, 7 ed., 1979.

[34] P. A. Durbin, "Perspectives on the phenomenology and modeling of boundary layer transition," *Flow, Turbulence and Combustion*, vol. 99, p. 1–23, 2017.

[35] M. V. Morkovin, "Bypass transition to turbulence and research Desiderata," NASA. Lewis Research Center Transition in Turbines, July 1985.

[36] R. E. Mayle and A. Schulz, "The path to predicting bypass transition," *Journal of Turbomachinery*, vol. 119, pp. 405–411, 07 1997.

[37] P. B. S. Lissaman, "Low-reynolds-number airfoils," *Annual Review of Fluid Mechanics*, vol. 15, no. 1, pp. 223–239, 1983.

[38] H. P. Horton, *Laminar separation bubbles in two and three dimensional incompressible flow.* PhD thesis, Queen Mary University of London, 1968.

[39] W. Saric, J. Ruben Carrillo, and M. Reibert, "Leading-edge roughness as a transition control mechanism," in *36th AIAA Aerospace Sciences Meeting and Exhibit*, January 1998.

[40] C. Sheng, *Advances in Transitional Flow Modeling: Applications to Helicopter Rotors*. SpringerBriefs in Applied Sciences and Technology, Springer, 2017.

[41] E. W. Warren and H. A. Hassan, "Alternative to the en method for determining onset of transition," *AIAA Journal*, vol. 36, no. 1, pp. 111–113, 1998.

[42] R. B. Langtry, *A Correlation-Based Transition Model Using Local Variables for Unstructured Parallelized CFD codes*. Ph.d. dissertation, Universität Stuttgart, Stuttgart, May 2006.

[43] H. W. Stock and W. Haase, "Navier-stokes airfoil computations with en transition prediction including transitional flow regions," *AIAA Journal*, vol. 38, no. 11, pp. 2059–2066, 2000.

[44] J. Sousa and L. Silva, "Transition prediction in infinite swept wings using navier–stokes computations and linear stability theory," *Computers & Structures*, vol. 82, no. 17, pp. 1551–1560, 2004. Computational Mechanics in Portugal.

[45] A. Krumbein, "Automatic transition prediction and application to high-lift multi-element configurations," *Journal of Aircraft*, vol. 42, no. 5, pp. 1150–1164, 2005.

[46] J. G. Coder and M. D. Maughmer, "Computational fluid dynamics compatible transition modeling using an amplification factor transport equation," *AIAA Journal*, vol. 52, pp. 2506–2512, Nov. 2014.

[47] R. C. Schmidt and S. V. Patankar, "Simulating boundary layer transition with low-reynolds-number k–ϵ turbulence models: Part 2—an approach to improving the predictions," *Journal of Turbomachinery*, vol. 113, pp. 18–26, 01 1991.

[48] X. Zheng, C. Liu, F. Liu, and C.-I. Yang, "Turbulent transition simulation using the k–ω model," *International Journal for Numerical Methods in Engineering*, vol. 42, no. 5, pp. 907–926, 1998.

[49] D. C. Wilcox, "Simulation of transition with a two-equation turbulence model," *AIAA Journal*, vol. 32, no. 2, pp. 247–255, 1994.

[50] R. Langtry and S. Sjolander, "Prediction of transition for attached and separated shear layers in turbomachinery," in *38th AIAA/ASME/SAE/ASEE Joint Propulsion Conference and Exhibit*, 2002.

[51] D. Walters and J. Leylek, "A new model for boundary layer transition using a single-point RANS approach," *Journal of Turbomachinery*, vol. 126, pp. 193–202, January 2004.

[52] D. Walters and D. Cokljat, "A three-equation eddy-viscosity model for reynolds-averaged navier-stokes simulations of transitional flow," *Journal of Fluids Engineering, Transactions of the ASME*, vol. 130, no. 12, pp. 1214011–12140114, 2008.

[53] R. Pacciani, M. Marconcini, A. Arnone, and F. Bertini, "Predicting high-lift low-pressure turbine cascades flow using transition-sensitive turbulence closures," *Journal of Turbomachinery*, vol. 136, p. 051007, 09 2013.

[54] S. Kubacki and E. Dick, "An algebraic model for bypass transition in turbomachinery boundary layer flows," *International Journal of Heat and Fluid Flow*, vol. 58, pp. 68–83, 2016.

[55] D. C. Wilcox, "Formulation of the k-w turbulence model revisited," *AIAA Journal*, vol. 46, pp. 2823–2838, November 2008.

[56] S. Kubacki, D. Simoni, D. Lengani, and E. Dick, "An extended version of an algebraic intermittency model for prediction of separation-induced transition at elevated free-stream turbulence level," *International Journal of Turbomachinery, Propulsion and Power*, vol. 5, no. 4, 2020.

[57] C. Seyfert and A. Krumbein, "Correlation-based transition transport modeling for three-dimensional aerodynamic configurations," in *50th AIAA Aerospace Sciences Meeting Including the New Horizons Forum and Aerospace Exposition*, 2012.

[58] S. Medida and J. Baeder, "A new crossflow transition onset criterion for rans turbulence models," in *21st AIAA Computational Fluid Dynamics Conference*, 2013.

[59] C. Grabe and A. Krumbein, "Extension of the model for prediction of crossflow transition," *52nd aerospace sciences meeting, AIAA SciTech Forum*, pp. 13–17, 2014.

[60] R. Langtry, "Extending the gamma-rethetat correlation based transition model for crossflow effects (invited)," in *45th AIAA Fluid Dynamics Conference*, 2015.

[61] P. Dassler, D. Kozulovic, and A. Fiala, "An approach for modelling the roughness-induced boundary layer transition using transport equations," *In:6th European congress on computational methods in applied sciences and engineering (ECCOMAS)*, pp. 10–14, 2014.

[62] U. Kaynak, "Supersonic boundary layer transition prediction under the effect of compresibilty using correlation based model," *Proc. IMechE, Part G*, vol. 226, no. 7, pp. 722–739, 2012.

[63] K. Lodefier, B. Merci, C. De Langhe, and E. Dick, "Transition modelling with the sst turbulence model and an intermittency transport equation," in *Turbo Expo: Power for Land, Sea, and Air*, vol. 5: Turbo Expo 2003, Parts A and B, pp. 771–777, 06 2003.

[64] K. Lodefier and E. Dick, "Modelling of unsteady transition in low-pressure turbine blade flows with two dynamic intermittency equations," *Flow, Turbulence and Combustion*, vol. 76, pp. 103–132, 2006.

[65] X. Ge, S. Arolla, and P. Durbin, "A bypass transition model based on the intermittency function," *Flow, Turbulence and Combustion*, vol. 93, no. 1, pp. 37–61, 2014.

[66] P. Durbin, "An intermittency model for bypass transition," *International Journal of Heat and Fluid Flow*, vol. 36, pp. 1–6, 2012.

[67] E. Juntasaro, K. Ngiamsoongnirn, P. Thawornsathit, and P. Durbin, "Development of an intermittency transport equation for modeling bypass, natural and separation-induced transition," *Journal of Turbulence*, vol. 22, no. 9, pp. 562–595, 2021.

[68] G. Walker and J. Gostelow, "Laminar-turbulent transition in boundary layers on axial turbomachine blades," *ERCOFTAC Bulletin*, vol. 80, pp. 11–15, September 2009.

[69] P. Jonáš, O. Mazur, and V. Uruba, "On the receptivity of the by-pass transition to the length scale of the outer stream turbulence," *European Journal of Mechanics - B/Fluids*, vol. 19, no. 5, pp. 707–722, 2000.

[70] M. Kato and B. Launder, "The modelling of turbulent flow around stationary and vibrating square cylinders," in *9th Symposium on Turbulent Shear Flows*, (Kyoto, Japan), pp. 10–4, August 1993.

[71] J. Sandhu and S. Ghosh, "Dynamical systems analysis of a zero-equation transition model," *AIAA Journal*, vol. 59, no. 10, pp. 4274–4280, 2021.

[72] P. Ströer, C. Grabe, and A. Krumbein, "Assessment and modification of the $\gamma - Re_\theta$ transition model behavior outside the boundary layer," in *New Results in Numerical and Experimental Fluid Mechanics XII* (A. Dillmann, G. Heller, E. Krämer, C. Wagner, C. Tropea, and S. Jakirlić, eds.), pp. 120–130, Springer International Publishing, 2020.

[73] G. B. Schubauer and P. S. Klebanoff, "Contributions on the mechanics of boundary-layer transition," NACA Technical Note TN-3489, 1955.

[74] E. A. Luke, X. Tong, and R. Chamberlain, "flowPsi: An ideal gas flow solver The User Guide," Jan. 2023.

[75] E. F. Toro, M. Spruce, and W. Speares, "Restoration of the contact surface in the HLL-Riemann solver," *Shock Waves*, vol. 4, pp. 25–34, July 1994.

[76] B. van Leer, "Towards the ultimate conservative difference scheme. V. A second-order sequel to Godunov's method," *Journal of Computational Physics*, vol. 32, pp. 101–136, July 1979.

[77] U. Goldberg, O. Peroomian, and S. Chakravarthy, "A wall-distance-free k-ϵ model with enhanced near-wall treatment," *Journal of Fluids Engineering*, vol. 120, pp. 457–462, 09 1998.

[78] R. McGhee, B. Walker, and B. Millard, "Experimental results for the eppler 387 airfoil at low reynolds numbers in the langley low-turbulence pressure tunnel," Technical Memorandum 4062, NASA, 1988.

[79] D. M. Somers, “Design and experimental results for a natural-laminar-flow airfoil for general aviation applications,” Technical Publication (TP) 1861, NASA, June 1981.

[80] D. Wilcox, “The remarkable ability of turbulence model equations to describe transition,” in *Fifth Symposium on Numerical and Physical Aspects of Aerodynamic Flows* (T. Cebeci, ed.), January 1992.

[81] K. Lodefier and E. Dick, “Transition modelling with an intermittency transport equation,” *ERCOFTAC Bulletin*, vol. 54, pp. 17–21, September 2002.

APPENDIX A

Re_θ PREDICTION USING LOCAL VARIABLES

Using vorticity (or shear) Reynolds number Re_v as a sign of transition is the major breakthrough in the development of intermittency based models. By this way, non-local operations to calculate a boundary layer parameter are avoided, and fully local formulations compatible with modern CFD techniques are made possible. Two different but related ways may be shown to support this relation. First one is based on the findings of Van Driest and Blumer [17] that breakdown of a laminar boundary layer is related to the high vorticity (shear) regions sufficiently away from the wall viscous damping. Langtry and Sjolander [50] showed that the maximum value of the laminar fluctuations are in great agreement with the maximum value of the vorticity Reynolds number Re_v, and those two parameters develop by showing almost the same profiles along the boundary layer as represented in Fig. A.1. Therefore, Langtry and Sjolander [50] came to a conclusion that local vorticity Reynolds number can be used as a sign of amplification of the disturbances in a laminar boundary layer. Then, they developed a low Reynolds number model that controls the transition onset using vorticity Reynolds number.

Second way to understand the relation between Re_θ and Re_v may be provided using boundary layer theory. Menter et al. [6] used $Re_v = Sy^2/\nu$ in non-dimensional $Re_v/(2.07Re_{\theta c})$ ratio as an indicator of transition onset in their early one equation γ transition model, but the detailed derivations were not given in the article, just giving reference to Wilcox [80] and saying that it is a direct result of the Blasius boundary layer solution. The solution given by Wilcox [80] is somehow hard to follow, so another paper will be presented here. Lodefier and Dick [81] analyzed the aforementioned parameter of Menter et al. [6], and provided a clear derivation based

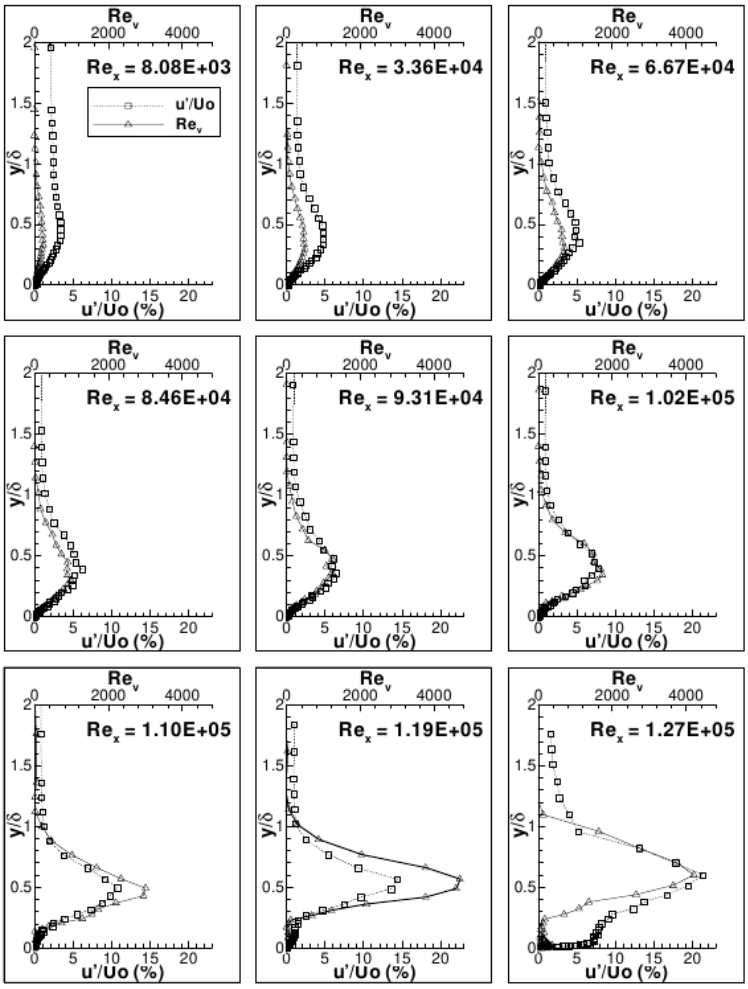

Figure A.1: Laminar fluctuations and local vorticity Reynolds number variations perpendicular to the wall. Reproduced from Langtry and Sjolander [50].

on Pohlhausen laminar boundary layer profiles.

Following derivation is taken from Lodefier and Dick [81].

Starting with

$$\frac{u}{U_\infty} = (2\eta - 2\eta^3 + \eta^4) + \lambda(2\eta - 6\eta^2 + 6\eta^3 - 2\eta^4) \tag{A.1}$$

where $\eta = y/\delta$, δ boundary layer thickness, λ pressure gradient parameter.

$$S = \frac{\partial u}{\partial y} = \frac{U_\infty}{\delta} \frac{\partial \left(\frac{u}{U_\infty} \right)}{\partial \eta} \tag{A.2}$$

$$\frac{Sy^2}{\nu} = \frac{U_\infty \delta}{\nu} \left[2 - 6\eta^2 + 4\eta^3 + \lambda \left(2 - 12\eta + 18\eta^2 - 6\eta^3 \right) \right] \eta^2 \tag{A.3}$$

Boundary conditions for $\frac{Sy^2}{\nu}$ is zero at the wall ($\eta = 0$) and freestream ($\eta = 1$). Then, in the boundary layer, it becomes maximum when

$$\eta = \frac{-1 + 8\lambda - \sqrt{21 - 36\lambda + 24\lambda^2}}{20\lambda - 10} \tag{A.4}$$

Inserting (A.4) into (A.3) gives

$$\begin{aligned} \left(\frac{Sy^2}{\nu} \right)_{max} &= \frac{U_\infty \delta}{\nu} f_1(\lambda) \\ &= Re_\theta \frac{\delta}{\theta} f_1(\lambda) \end{aligned} \tag{A.5}$$

where θ is the momentum thickness.

Based on (A.1), they find

$$\frac{\delta}{\theta} = \frac{315}{37 - 4\lambda - 5\lambda^2} \tag{A.6}$$

Then, (A.5) becomes

$$\frac{\left(\frac{Sy^2}{\nu} \right)_{max}}{Re_\theta} = f_1^*(\lambda) \tag{A.7}$$

Also

$$K = \frac{\nu}{U_\infty^2} \frac{dU_\infty}{dx} = Re_\theta^{-2} \frac{\theta^2}{\nu} \left(-\frac{1}{\rho U_\infty} \frac{dp}{dx} \right) \tag{A.8}$$

Near the wall

$$\frac{dp}{dx} = \left(\frac{\partial \tau}{\partial y}\right)_0 = \mu \left(\frac{\partial^2 u}{\partial^2 y}\right)_0 = \mu \left(\frac{U_\infty}{\delta^2} 12\lambda\right) \tag{A.9}$$

Combining (A.8) and (A.9)

$$K\left(Re_\theta\right)^2 = \left(\frac{\theta}{\delta}\right)^2 12\lambda = f_2(\lambda) \tag{A.10}$$

Numerical fit of (A.7) and (A.10) results in

$$\frac{\left(\frac{Sy^2}{\nu}\right)_{max}}{Re_\theta} = 2.2 - \frac{20}{3} K\left(Re_\theta\right)^2 \tag{A.11}$$

They justify $K\left(Re_\theta\right)^2$ term is negligible small, and then finally

$$\left(\frac{Sy^2}{2.2\nu}\right)_{max} = Re_\theta \tag{A.12}$$

Later, the relation between Re_v and Re_θ was shown by Menter et al. [5] using Fig. A.2 and Fig. A.3. In addition to the equity of scaled $(Re_v)_{max}$ and Re_θ, the relative error between those is less than 10% for moderate pressure gradients. So, using Re_v instead of Re_θ provides an important tool in transition modeling.

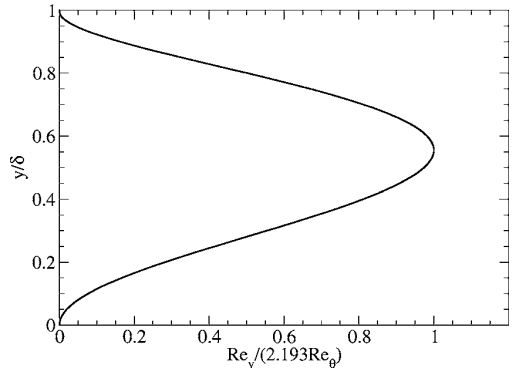

Figure A.2: Scaled vorticity Reynolds number Re_v profile in a Blasius boundary layer. Reproduced from Menter et al. [5].

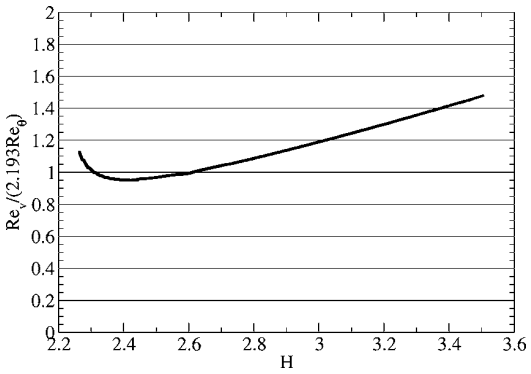

Figure A.3: Relative error between Re_v and Re_θ as a function of boundary layer shape factor H. Reproduced from Menter et. al. [5].